Global and Planetary Change 137 (2016) 88–106

Contents lists available at ScienceDirect

Global and Planetary Change

journal homepage: www.elsevier.com/locate/gloplacha

The impact of climate change on the global coastal low-level wind jets: EC-EARTH simulations

Alvaro Semedo [a,b,*], Pedro M.M. Soares [b], Daniela C.A. Lima [b], Rita M. Cardoso [b], Mariana Bernardino [c,d], Pedro M.A. Miranda [b]

[a] Escola Naval-CINAV, Lisbon, Portugal
[b] Instituto Dom Luiz, Faculdade de Ciências, University of Lisbon, Lisbon, Portugal
[c] IPMA-Instituto Português do Mar e da Atmosfera, Lisbon, Portugal
[d] Centre for Marine Technology and Engineering (CENTEC), Instituto Superior Técnico, Universidade de Lisboa, Lisbon, Portugal

ARTICLE INFO

Article history:
Received 27 March 2015
Received in revised form 16 November 2015
Accepted 15 December 2015
Available online 17 December 2015

Keywords:
Coastal jets
Coastal low level jets
EC-Earth
Climate change
Regional climate

ABSTRACT

Coastal low-level jets (CLLJ) are low tropospheric coast-parallel wind features, confined to the marine atmospheric boundary layer, which lay on the east flank of the semi-permanent sub-tropical high-pressure systems, in the mid-latitudes, along equator-ward eastern boundary currents. Coastal jets are of utmost relevance to the regional climate, through their impact on the along coast sea surface temperature, driving the upwelling of cold deep nutrient-rich waters, and by having a decisive impact on the aridity of the mid-latitude western coastal areas. Here the impact of a warmer climate in the CLLJ climate is investigated, through a 2-member ensemble of EC-Earth CMIP5 simulations of future climate, following the RCP8.5 greenhouse gases emissions scenario. Besides the projected changes of the CLLJ, towards the end of the 21st century, the future characteristics of the coastal jets are also presented. No common feature of projected changes in the seven identified CLLJ areas was identified. The Iberian Peninsula and the Oman coastal jets are the ones that presented the highest differences, compared to present climate: highest projected increases in frequency of occurrence, as well as highest projected increases in jet strength (wind speed at the jet height) and jet height. This study presents a step forward towards a larger ensemble of CLLJ projections, required to better assess robustness and uncertainty of potential future climate change.

1. Introduction

There is a broad scientific consensus that the warming exhibited during the twentieth century climate has been caused by the enhancement of greenhouse gases concentration in the atmosphere caused by anthropogenic emissions (IPCC, 2013). Due to the inertia of the Earth climate system, but also due to expected additional greenhouse gases emissions, it is expected that the climate will continue to warm, at least until the end of the 21st century (Solomon et al., 2007).

Coastal low-level jets (henceforth referred to as "coastal jets" or simply as CLLJ) are low tropospheric coast-parallel wind features, with wind speed maxima confined to the marine atmospheric boundary layer (MABL), typically below ~1000 m (most of the times below ~500 m) above sea level (ASL; e.g. Beardsley et al., 1987, Garreaud and Muñoz, 2005, Ranjha et al., 2013). Although having a low vertical extent, CLLJ have a large horizontal span offshore, to distances of the order of hundreds of kilometers (e.g. Winant et al., 1988, Muñoz and Garreaud, 2005, Soares et al., 2014, Ranjha et al., 2015a).

Coastal jets lay on the east flank of the semi-permanent sub-tropical high-pressure systems, in the mid-latitudes, along equator-ward eastern boundary currents (EBC; Winant et al., 1988, Ranjha et al., 2013): along the California and Canary currents, in the northern hemisphere, and along the Peru-Humboldt, Benguela and West Australia currents in the southern hemisphere (Fig. 1 below). The high pressure systems over the ocean, along with thermal low pressure patterns in-land, provide the synoptic forcing behind CLLJ occurrences. An exception is the Oman CLLJ, in the Arabian Sea, where the intricate interaction between the Summer South Asia Monsoon and the Findlater jet (also known as Somali jet; Findlater, 1969) forces a coastal jet feature off the southeast coast of Oman (Ranjha et al., 2015a). The Oman CLLJ is the only one that does not occur along an EBC in a western continental coast, in the mid-latitudes, its lower latitude (hence a low magnitude of the Coriolis force) and the northward migration of the inter-tropical convergence zone to the Indian sub-continent during summer (Gergana et al., 2007), give particular characteristics to the Oman coastal jet. In fact two low-level jets coexist in the area: the Oman CLLJ, close to the sea surface along the Yemen-Oman coasts, and the Findlater or Somali jet, which is not a coastal jet, at a higher altitude (Ranjha et al., 2015a).

Ranjha et al. (2013) produced a global climatology of coastal jets from ERA-Interim data (Dee et al., 2011), showing that CLLJ occur

* Corresponding author at: Escola Naval-CINAV, Base Naval de Lisboa, Alfeite, 2810-001, Almada, Portugal.
E-mail address: milho.semedo@marinha.pt (A. Semedo).

http://dx.doi.org/10.1016/j.gloplacha.2015.12.012
0921-8181/

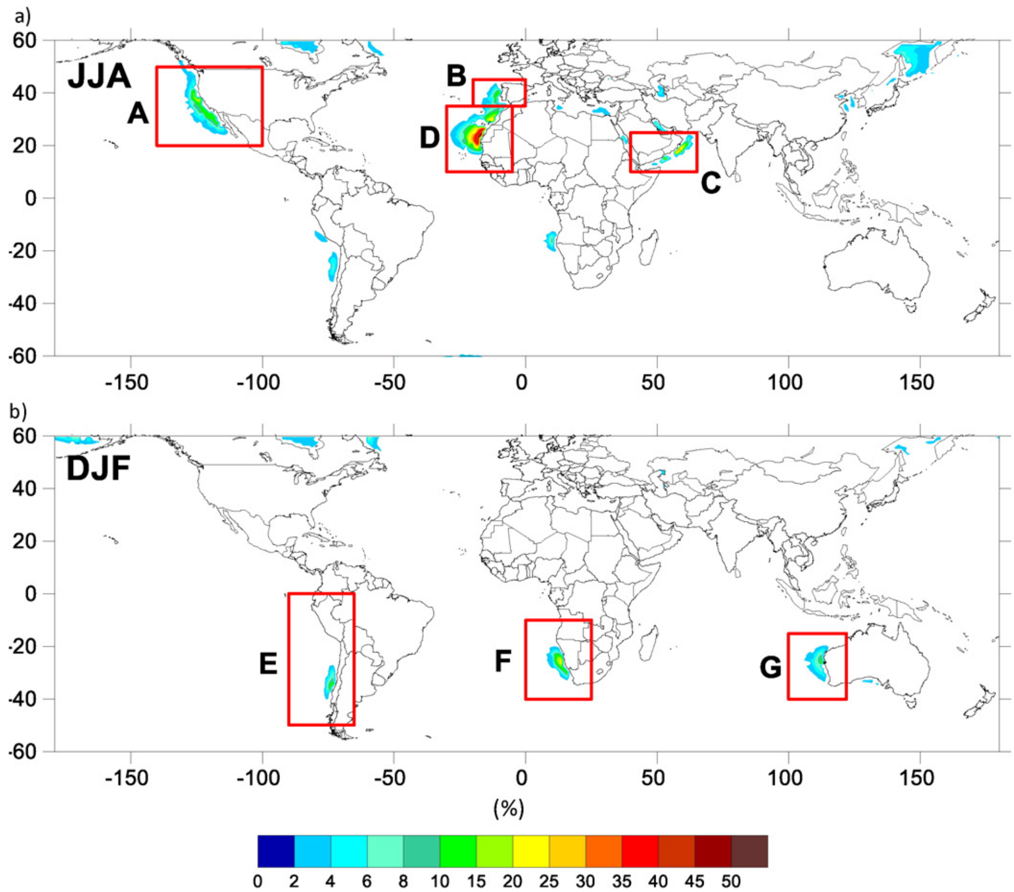

Fig. 1. Ensemble global maps of CLLJ frequency of occurrence (%) for (a) JJA and (b) DJF. Coastal jets regions of interest enclosed in red, A — California CLLJ, B — Iberian-Peninsula CLLJ, C — Oman CLLJ, D — West Australian CLLJ, E — Peru-Chile CLLJ, F — North-African CLLJ and G — Benguela CLLJ.

mainly in summer, and to a certain extend in spring and early fall (see also Soares et al., 2014). They have also shown that the intra-annual variation of coastal jets is lower in the southern hemisphere, particularly in the Benguela jet, that, in spite of some meridional variation, can occur all year round (Nicholson, 2010). The coast parallel winds associated with coastal jets are responsible for coastal upwelling due to offshore Ekman transport, bringing cold deep water to the surface, decreasing the sea surface temperature (SST) along the coast and sharpening the ocean-land thermal (and pressure) difference. The sharp thermal and pressure gradients are therefore higher at the coast, decreasing off-shore and inland (Zemba and Friehe, 1987, Winant et al., 1988).

The warm and dry subsiding air above, from the sub-tropical high-pressure and the cold marine air at the surface, set sharp temperature and humidity inversions that cap the MABL close to the coast, constraining the CLLJ wind speed maxima at lower altitudes. The decreasing temperature of the marine layer close to the coast is ultimately responsible for the sloping of the capping inversion towards the coast. The thermal wind associated with CLLJ is a result of this sloping of the MABL height towards the coast. The increase of the wind speed near-shore is therefore the result of channeled flow, with a squeezed MABL in the vertical, a pressure gradient towards the coast, and a mechanical constraint imposed by coastal topography (Winant et al., 1988, Burk and Thompson, 1996, Burk et al., 1999, Tjernström and Grisogono, 2000) and by the structure of the coastlines (Burk and Thompson, 1996), in a flow regime that is comparable with a reduced gravity flow in a two layer hydraulic system (Tjernström and Grisogono, 2000). The wind speed is highest in altitude due to surface friction (reducing the wind speed at the surface). The vertical wind shear induces mechanically produced turbulence inside the MABL, that leads to a well mixed coastal boundary layer. The MABL in a coastal jet environment is therefore typically moist, well mixed, stable, and cool, due to the influence of the low SST. In spite of its synoptic scale forcing this local intensification of the ocean-land thermal contrast and local high wind speeds is what makes coastal jets mesoscale wind features. Coastal topography and its orientation in relation to the flow can also result in additional local enhancement of the wind speed. If coastal mountains are higher than the MABL the lateral (cross-shore) wind component is blocked. This blocking channels the flow and is responsible for further increases of the wind speed (Winant et al., 1988, Burk and Thompson, 1996, Tjernström and Grisogono, 2000). The wind speed and direction can also be affected by points and capes through a process called expansion fan (Burk and Thompson, 1996). This increase in the wind speed has a direct impact on the local SST (through the enhancement of the upwelling) and cloud cover in the lee of headlands (Nuss et al., 2000).

Coastal jets are an important feature of the regional climates of the mid-latitude western continental regions. Low SST along the coast, due to upwelling, lowers the evaporation over the ocean and the strong coast parallel winds limit the advection of marine air in-shore, considerably limiting the water vapor content over land. Hence some of the mid-latitude western coastal regions, like the Namib or Atacama deserts, are within the most arid areas of the planet (Warner, 2004). The MABL dynamics at the coast is strongly linked to the marine cloud formation (low stratiform clouds and fog; Olivier, 1995; Nuss et al., 2000, Koracin and Dorman, 2001, Tjernström and Koračin, 1995). The influence of coastal winds and CLLJ on the inland water vapor content has also an impact on cloud formation and the radiative balance there.

Coastal jets are strongly linked to regional ocean dynamics, with impacts in the atmosphere and the ocean (Beardsley et al., 1987), forcing coastal upwelling and nutrient-enriched waters at the coast. The major upwelling zones occur along EBC, and are among the most productive regions of the global ocean: 17% of the worldwide fish captures take place along the coastal upwelling regions (Pauly and Christensen, 1995). Future changes in CLLJ and in coastal winds along EBC will have a direct impact on the upwelling regimes, and consequently on the biological production within the continental shelves and on the regional climates of the mid-latitude western continental areas. The greenhouse warming is expected to lead to a lower night-time cooling and to an enhancement of the daytime heating, due to less in-land water vapor content and to the intensification of the continental thermal lows in the western continental regions. This intensification can, in turn, change the synoptic forcing pattern of the CLLJ, intensify the alongshore wind speed and change the upwelling circulations. The cooling of the coastal SST can further lead to higher coastal wind speeds, less water vapor advection in-land, with consequences on the coastal marine clouds and to the in-land radiative budget. The need of a comprehensive study of the impact of climate change on coastal jets is therefore paramount. In recent years there have been several studies, although not conclusive, concerning the sensitivity of coastal upwelling to climate change (e.g. Bakun, 1990, Snyder et al., 2003, Demarcq, 2009; Narayan et al., 2010, Miranda et al., 2013). Studies on the impact of the overlaying wind responsible for the upwelling are nevertheless scarce, and none has tackled the future climate of coastal jets, which is the main goal of this study.

By using the classification and filtering criteria of CLLJ established by Ranjha et al. (2013), the impact of a warmer climate on the global coastal jets occurrences and characteristics in the 21st century is analyzed here. The study is based on a 2-member global climate model (GCM) EC-Earth Coupled Model Intercomparison Project Phase 5 (CMIP5) runs (henceforth also referred to as “ensemble”). A twentieth century period (1971–2000) from present climate is used as control (or historic) run. The ensemble reference period (the control run) is evaluated against remote sensing wind speed observations and compared to the European Centre for medium-range weather forecasts (ECMWF) ERA-Interim reanalysis. The projected changes in the global CLLJ climate towards the end of the 21st century are analyzed for the 2071–2100 period.

The paper continues in Section 2, where the EC-Earth model is presented, along with the methodology used to assess the occurrence of CLLJ. Subsequently in Section 3 the results of the control run are evaluated against remote sensing wind speed data and ERA-Interim data, for present-day conditions. The global results of the impact of climate change on the global CLLJ pattern are presented in Section 4. In Section 5, the results are summarized and the concluding remarks along with suggestions for further research are presented.

2. Model, data and methodology

2.1. Global climate model

The EC-Earth model is a full physics seamless atmosphere–ocean-sea-ice coupled earth system prediction model (Hazeleger et al., 2010), developed from the operational seasonal forecast system of ECMWF. The version 2.2 used here is based on the ECMWF seasonal forecast system 3 (http://www.ecmwf.int/products/forecasts/seasonal/documentation/system3/index.html;

last access on December 31, 2014). The atmospheric model in EC-Earth is the ECMWF Integrated Forecast System (IFS) cycle 31r. The set-up of the atmospheric model in the EC-Earth version 2.2 corresponds to the use of a horizontal spectral resolution of T159 (triangular truncation at wavenumber 159), roughly 125 km, and a vertical grid with vertical 62 levels of a terrain-following mixed sigma-pressure hybrid coordinates, of which about 15 are within the planetary boundary layer (PBL). The PBL scheme used in the simulations is the EDMF (Eddy Diffusivity Mass Flux scheme). The lowest model level is at 30 m height above the surface, and the highest level is at 5 hPa. The ocean model is the Nucleus for European Modeling of the Ocean (NEMO), developed by Institute Pierre Simon Laplace using a horizontal resolution of roughly one degree. The temporal output sampling of the EC-Earth simulations is 6 h. The performance of the EC-Earth has been addressed in different studies regarding the atmosphere (e.g. Hazeleger et al., 2013) and the ocean (e.g. Sterl et al., 2012) model components. Hazeleger et al. (2013) has shown that the EC-Earth model simulates well the tropospheric fields and the dynamic variables, and worse the surface temperature and fluxes. Sterl et al. (2012) showed that the ocean component of EC-Earth has a reasonable performance, emphasizing that in general the model has a cold and fresh (low salinity) bias, but that in the Southern Ocean a strong warm SST bias is present.

Two CMIP5 EC-Earth simulations (the ensemble members) are used in the present study. The two ensemble members' past-present climate simulations were initialized in 1850 and 1855. The past and present climate simulations cover the period between1850 and 1855 to 2005, and the future climate runs span from 2006 to 2100, following the representative concentration pathway (RCP) with a high emissions scenario 8.5 (RCP8.5; Riahi et al., 2011). The present climate twentieth century period (1971–2000) is used as control (historic) run. The projected changes in the global CLLJ climate in the future, due to the impact of a warmer climate, are analyzed for the 2071–2100 period.

2.2. Methodology

The present study uses the CLLJ identification method from Ranjha et al. (2013), where a set of filtering criteria, based on the analysis of the wind-speed and temperature vertical profiles were proposed. A positive detection of a CLLJ occurrence will happen when the following criteria are satisfied:

- The height of the jet maximum is within the lowest 1 km;
- The wind speed at the jet maximum is at least 20% higher than the wind speed at the surface;
- The wind speed above the jet maximum decreases to below 80% of the wind speed at the surface (i.e. a 20% falloff) before reaching 5 km above its maximum;
- The temperature at the jet maximum is lower than the temperature at two model levels above it (inversion detection); and
- The maximum temperature does not occur at the base (rejection of surface based inversion).

These criteria were applied sequentially to the wind speed and temperature vertical profiles of the two ensemble members, at each grid point, to identify the location of coastal jets occurrences, and further compute the frequency of occurrence of CLLJ and its climatological characteristics, for the control run and future periods. The horizontal wind speed was calculated from the u and v wind components. The assessment of the impact of climate change on CLLJ occurrences and properties (coastal jet height and wind speed at the jet height) is based on the comparison between the historic and future results of the ensemble.

A first step in evaluating the ensemble control runs, by comparing its results with remote sensing observations, is required, so that subsequently the study can rely on the assumption that the GCM will perform similarly for future conditions (Knutti, 2008). In the comparisons with the remote sensing observations and ERA-Interim reanalysis data the time constraint is ignored, since the EC-Earth integrations were not subject to data assimilation, and they are considered as representative of the present-day climatological mean atmospheric conditions, regardless of the time period. Hence, the comparisons were made between the GCM runs period (1971–2000), and the ERA-Interim period (1979–

2012) and remote sensing data time-slice (1987–2011), by averaging the three data sets into Julian years. The 6-hourly gridded parameters were processed to the December–February (DJF), March–May (MAM), June–August (JJA), and September–November (SON) seasons. Here we focus only on the "extreme" DJF and JJA seasons (the austral and boreal summers, although in some situations the respective winters are also analyzed).

2.3. Evaluation data: ERA-Interim and remote sensing observations

ERA-Interim is a third generation reanalysis of meteorological observations produced by ECMWF. The ongoing project was supposed to go back only to 1989, but in 2011 the reanalysis was extended further backwards to 1979. Here we use the period from January 1979 to December 2012. Besides atmospheric variables, the ERA-Interim also includes wave parameters, since it was produced using the IFS (Integrated Forecasting System; release cycle Cy31r2, used operationally at ECMWF during the period December 2006 through June 2007), a two-way coupled atmosphere-wave model system (Janssen, 2004). The horizontal resolution of the atmospheric model is approximately 79 km (T255 spectral truncation) on a reduced Gaussian grid. The temporal resolution of ERA-Interim is 6 h. Additional details about the ERA-Interim reanalysis can be found in Dee and Uppala (2009) and Dee et al. (2011).

The remote sensing observations used to evaluate the ensemble members' surface wind fields are based on the Cross-Calibrated Multi-Platform (CCMP) Ocean Surface Wind Vector Analyses (Atlas et al., 2011). These winds are made available by NASA (National Aeronautics and Space Administration), and were obtained from a number of microwave satellite instruments. The global dataset spans from July 1987 to June 2011 without gaps, merging cross-calibrated satellite winds using a variational analysis method. The surface wind refers to 10 m height daily mean winds at 0.258° horizontal resolution in a regular grid. The CCMP wind data have been compared against in situ wind speed observations from several ocean moored buoys, revealing good agreement with (within 0.8 m/s), regardless of the different instrument wind retrieval measurement dynamics procedures. The EC-Earth 10 m wind fields were compared with the referred observations through a nearest point approach, for the observational time-slice.

3. Model evaluation in the control run reference period

3.1. Statistical evaluation

The areas where CLLJ were found by Ranjha et al. (2013) are presented in Fig. 1 (red dashed line): in the northern hemisphere, off the coasts of California-Oregon (California CLLJ; box A), off the coasts of West Iberia (Iberian Peninsula CLLJ; box B) and Northeast Africa (North-African CLLJ; box F), and in the southern hemisphere, off the coasts of Peru-Chile (Peru-Chile CLLJ; box E), off the coasts of Namibia-Angola (Benguela CLLJ; box G), and off the coast of West Australia (West Australia CLLJ; box D). Fig. 1 also depicts the area off the southeast coast of the Arabian Peninsula, where the Oman coastal CLLJ (box C) has also been described by Ranjha et al. (2013, 2015a).

Each (control run) ensemble member 10 m wind speeds were compared to the CCMP 10 m wind speeds inside the CLLJ. The observational grid points (not coincident with EC-Earth) were linked to the EC-Earth's nearest grid point. Near the shore the observational dataset has a significant number of missing values, thus grid points with less than 95% of data were dismissed.

The following statistics have been computed: in each box, all the grid points were pooled together to determine the bias, the mean absolute error (MAE), the mean absolute percentage error (MAPE), the root mean square error (RMSE), and the correlation coefficient (computed for Julian years for each data set; see Soares et al., 2012 and Cardoso et al., 2013 for additional details). Table 1 shows the values of these statistics for each ensemble member, in each of the box areas. The EC-Earth ensemble members have similar global error measures in all areas, with no significant differences between them. The low MAE and MAPE show that the modeled wind speed is in good agreement with the observational dataset. Overall, MAE is less than 1 ms^{-1}, representing 10 to 17% of the observed mean wind speed. The bias has a greater variability between regions and is lower than the MAE which, along with the higher RMSE, is indicative of the existence of high deviations from the observations that cancel each other out. This is more significant in the Australian West Coast, with a -0.01 ms^{-1} bias, while the mean average error is 0.86 ms^{-1} and the RMSE is 1.25 ms^{-1}. The area with higher errors is the one along the southeast coast of the Arabian Peninsula, but in contrast, it has the highest correlation with the observations. The correlation shows a higher dissimilarity between regions but, nevertheless, high correlations are obtained in all regions.

Table 1
Global error statistics of surface wind speeds of the two EC-EARTH ensemble members.

	Bias (m/s)	MAPE (m/s)	MAPE (%)	RMSE (m/s)	CORR
CCJ	0.11/0.07	0.70/0.72	10.46/10.67	1.13/1.15	0.75/0.75
IPCJ	0.21/0.20	0.88/0.90	11.94/12.18	1.14/1.16	0.55/0.55
OCJ	0.59/0.64	0.98/1.01	16.45/16.83	1.29/1.32	0.91/0.91
NACJ	0.34/0.34	0.91/0.95	13.68/14.35	1.14/1.19	0.63/0.56
PCCJ	0.14/0.16	0.79/0.79	11.40/11.30	1.10/1.09	0.80/0.81
BCJ	0.17/0.20	0.90/0.89	12.43/12.30	1.30/1.30	0.68/0.68
WACJ	−0.01/−0.03	0.86/0.84	11.52/11.23	1.25/1.19	0.76/0.75

The EC-Earth ensemble wind speeds at two constant pressure levels within the MABL (925 and 850 hPa) were compared to ERA-Interim wind speeds in each box areas shown in Fig. 1. The ERA-Interim wind speeds were interpolated to the EC-Earth grid points. The JJA and DJF ensemble control run and the ERA-Interim wind speeds probability density functions (PDF), at the two pressure levels, were computed. The ensemble's ability to depict the wind speeds (as described by ERA-Interim) is summarized through the computation of two PDF scores following Perkins et al. (2007). The PDF skill score is based on the common overlap of the ensemble and reanalysis PDF. Firstly, the 90th percentile of the reanalysis winds is determined, secondly the PDF for the wind speed between 0 m/s and the 90th reanalysis percentile is calculated for both (ensemble and ERA-Interim), and thirdly the PDF for wind speed above the 90th percentile is determined. The two parts are then normalized separately and the degree of PDF overlap is calculated for each part then averaged (S), this gives an extra weight to the PDF tail, related to extreme. The skill score has values ranging from zero, for no overlap, and one hundred, for a perfect overlap.

Here we show this score as well as the fractional score for wind speeds bellow ERA-Interim's 90th percentile for the two pressure levels for JJA and DJF for all CLLJ areas (S and S < P90 respectively in Table 2). The overlap between the PDF, for all coastal regions, is higher, although marginally, at 850 hPa. Nevertheless, the scores are higher than 80%, except in the Iberian Peninsula region at 925 hPa and Peru region at 850 hPa, showing the good agreement, between the EC-Earth and Era-Interim winds inside the MABL. This agreement is even higher for

Table 2
DJF and JJA S and S < P90 wind speed PDF matching skill scores at the 925 hPa for the different CLLJ areas.

	DJF		JJA	
	S	S < P90	S	S90
CCJ	84.7	89.3	89.4	90.1
IPCJ	79.8	89.0	77.2	80.6
OCJ	82.8	83.2	88.0	92.8
NACJ	90.8	89.4	86.1	85.1
PCCJ	80.2	89.5	84.0	91.3
BCJ	90.4	95.7	83.5	90.9
WACJ	84.2	89.4	83.5	96.8

winds bellow the 90th percentile, where several regions have values above 90%.

3.2. Control run CLLJ fields

After having the ensemble wind speed and temperature vertical profiles filtered by the detection algorithm, at each grid point, global seasonal maps of CLLJ occurrences (in percentage) for JJA and DJF were produced, and are also presented in Fig. 1. These maps show, overlaid with the CLLJ areas, the percentage of time that coastal jets were positively identified at each grid point, out of the total number of data outputs in the ensemble, from 1971 to 2000 (22,080 in JJA and 21,664 in DJF). A visual inspection of the global JJA and DJF CLLJ occurrences allows the conclusion that EC-Earth, in spite of its coarse resolution, is capable of resolving CLLJ in coastal areas along EBC in both hemispheres. False positives in the Yellow Sea, in the Sea of Okhotsk, and in the Mediterranean seas, also present in Ranjha et al. (2013), should be ignored. While, from a global perspective, the structure and the seasonality, as well as the meridional migration of coastal jets are well captured by the ensemble, the values of the frequency of occurrence are lower than the values obtained from ERA-Interim by Ranjha et al. (2013); their Fig. 2). Although the pattern is similar to ERA-Interim, EC-Earth underpredicts coastal jets, compared to the reanalysis. This can be linked to the coarser resolution, but also, possibly, to the warm SST bias along EBC (Sterl et al., 2012) that EC-Earth is known to have. The largest differences are (for the respective hemisphere summer) in the California CLLJ (15%), and in the Oman CLLJ (also around 15%), and in the Benguela CLLJ(around 10%). The ensemble results for the Iberian Peninsula and North Africa coastal jets, as well as for the West Australia CLLJ are, on the other hand more comparable to the ERA-Interim ones.

The DJF and JJA ensemble mean sea level pressure (MSLP) and 10 m wind speeds (and directions) patterns, from the control run, are presented in Figs. 2 and 3, respectively. The MSLP seasonal patterns are well represented by the ensemble, namely the high vs. low pressure systems, over the ocean and in-land, along the mid-latitude western continental coasts (as well as the monsoon pressure pattern), responsible for the CLLJ occurrences. The ensemble JJA and DJF MSLP fields (Fig. 2a,b) compare rather well with ERA-Interim MSLP ones (not shown), although the semi-permanent high pressure fields are slightly deeper (around 1 hPa) in the ensemble. The seasonal 10 m wind speed patterns (as well as the wind directions) shown in Fig. 3a,b are also well resolved in the ensemble control run, compared to ERA-Interim (also not shown). As can be seen the intensification of the wind speeds, in summer, along the EBC (as well as in the Arabian Sea along the JJA Somali Current), as a consequence of the synoptic scale geostrophic adjustment, is well noticeable.

The agreement between the ensemble control run and the ERA-Interim wind speeds, at two pressure levels, and the remote sensing surface wind speed observations, in the CLLJ areas, as well as the ensemble coastal jets frequencies of occurrence MSLP and 10 m wind speed and direction patterns, show that the EC-Earth is capable of producing realistic results of coastal winds climate and CLLJ occurrences at end of the twentieth century, and to simulate a realistic climate change signal towards the end of the 21st century.

4. Climate change signals in the global CLLJ pattern

4.1. Changes in the CLLJ climate towards the end of the twenty-first century

The ensemble JJA and DJF global maps of CLLJ frequency of occurrence anomalies (frequency of occurrence differences, in percentage:

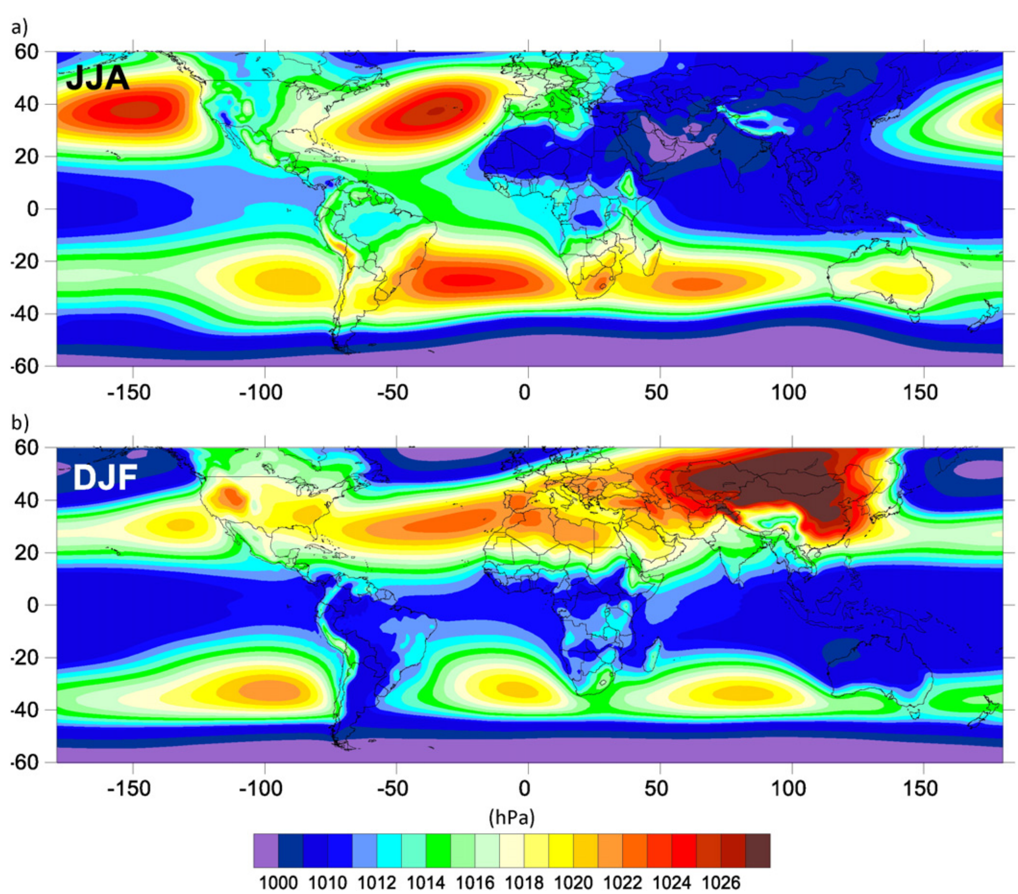

Fig. 2. Control run (1971–2000) ensemble global maps of MSLP (hPa) for (a) JJA and (b) DJF.

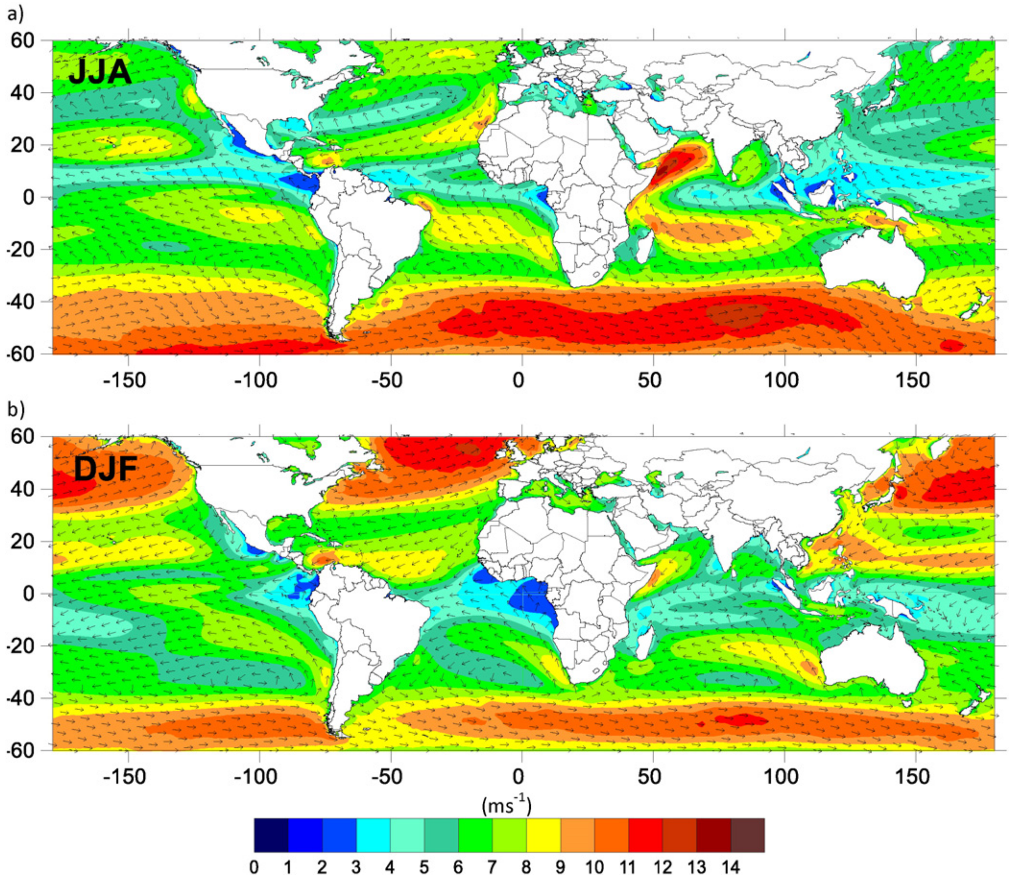

Fig. 3. Same as in Fig. 3 but for 10 m ASL wind speed (ms^{-1}) for (a) JJA and (b) DJF. Arrows represent the wind direction (not scaled with the background field).

future minus present) are shown in Fig. 4. A student-t statistical significance test was applied to the frequency of occurrence differences and the shading show the non-statistically significant anomalies at 95% confidence level. The projected changes towards the end of the 21st century show an increase in CLLJ occurrences in the northern hemisphere in JJA (Fig. 4a), mostly in the Iberian Peninsula CLLJ (8–10% increase, and higher than 10% off the coast of central Portugal), and in the Oman CLLJ (higher than 10%). Weaker future increases in the JJA occurrences of the California CLLJ (2–3%) are expected to take place. A summer and winter increase in the frequency of occurrence of the North Africa CLLJ is also projected to occur. In the boreal winter, considering that the frequencies of occurrence of the North Africa CLLJ shown in Fig. 1b are close to zero, a coastal jet is expected to develop in the future, offshore Cape Blanco, in Senegal. A low frequency of occurrence of the North Africa CLLJ in winter had already been identified by Ranjha et al. (2013) in the same area, hence an increase in the winter occurrences is likely to be expected. The projected differences in CLLJ occurrences in the southern hemisphere are lower than the northern hemisphere ones, nevertheless light increases (2–3%) of the southern hemisphere coastal jets during the austral summer (Fig. 4b) are also to be expected. Austral winter anomalies (differences) of the Peru-Chile and Benguela coastal jets (1–2% increases/decreases) are also shown.

4.2. Regional CLLJ changes analysis

A detailed examination on the future climate of each regional coastal jet is presented in Figs. 5 to 14). Detailed statistics of the projected changes of the jet height (the height of the wind speed maxima) and of the wind speed at that height, for the control run and for the ensemble future projections (for the end of the 21st century but also for a mid century time-slice: 2041–2070), are presented. The mid century projections are presented, in spite of the focus being the end of the mid century, to allow a perspective on the evolution of the CLLJ heights and wind speed. The projected changes for this period will be mentioned only when appropriate. The characteristics of the future CLLJ summer climate (for the 2071–2100 time slice) are also presented. For the coastal jets that have a significant yearly prevalence (North Africa, Peru-Chile, and Benguela coastal jets), the winter projected changes and future climate are shown together. Across-coast cross-sections of the mean wind speed and thermal structure, through the regions of future (late 21st century) maximum jet frequency of occurrence are shown. The cross-sections present the seasonally averaged wind speeds and isentropes when coastal jets occur.

4.2.1. California coastal jet

The regional analysis of the ensemble projected changes of the boreal summer California CLLJ heights and wind speed maxima are described in Fig. 5a,b histograms. A tendency towards future higher and with higher wind speeds, particularly for extreme wind speed events (higher than 20 ms^{-1}), is expected to occur by the mid and end 21st century, with less occurrences of lower height jets and of lower wind speeds. By the end of the 21st century, more than 50% of the California coastal jets are expected to be concentrated between 400 and 700 m ASL. The projected changes for the California CLLJ frequency of occurrence are presented in Fig. 5c as the ratio between the ensemble future (end of the century time slice: 2071–2100) and control run frequencies of occurrence (future divided by present). Increasing (decreasing) frequencies of occurrence are represented by values higher (lower) than

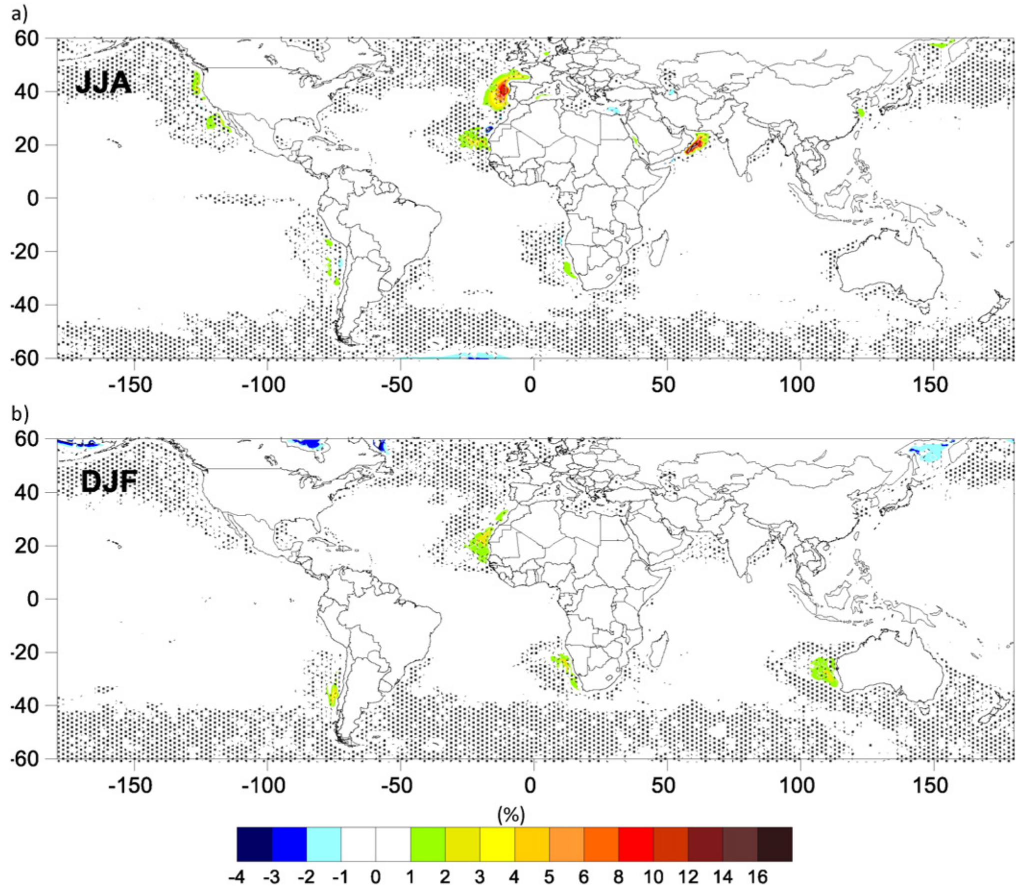

Fig. 4. Ensemble global maps of CLLJ frequency of occurrence anomalies (%; future minus present) for (a) JJA and (b) DJF. Frequency of occurrence differences: future (2071–2100) minus present (control run; 1971–2000). Shaded areas are non-statistically significant areas at 95% (student-t test).

1. These maps (shown here and in Figs. 6-14) are, to a certain extent, a regional magnification of Fig. 4, with increasing detail. Increases in the frequency of occurrence of the California CLLJ are expected to occur along the coasts of Washington and Oregon, down to Cape Mendocino (20–40%), and Baja California (slightly less). On the other hand, a reduction is projected to occur along Central California coast (20–30%).

The future California CLLJ wind direction, at the jet height, as projected by the ensemble, will be mostly from the north to north-northwest (more than 50% of the times; Fig. 5d), with eventually no changes from present climate (not shown). The height-wind speed histogram (Fig. 5e) shows that in the future the California coastal jets are expected to be concentrated between 400 to 600 m ASL, with wind speeds between 8 to 12 ms^{-1}. The future height of the CLLJ wind speed maxima is, to a good extend, a proxy of the MABL height, since the jet core is lodged right below the capping inversion (Burk and Thompson, 1996). Higher coastal jet wind speed maxima and MABL height may well be a representation of a warmer boundary layer, most probably related to higher SST due to a general increase of the ocean temperature. The east–west cross section of the seasonally averaged expected wind speeds (and isentropes), when jet occurs, is shown in Fig. 5f (along the black east–west line shown in the map in Fig. 5c; chosen here and for the remaining coastal jets across the area where the occurrences are highest). The future jet core will be at around 450 m ASL, with wind speeds higher than 13 m ms^{-1}, with an offshore span of the order of 200 km.

4.2.2. Iberian Peninsula coastal jet

Fig. 6 depicts the JJA Iberian Peninsula CLLJ projected changes and its characteristics for the future. The Iberian Peninsula coastal jet, together with the North Africa one, lays along the equator-ward Canary EBC system, which is unique, in the sense that it is disrupted by the influx of Mediterranean (denser) water, that sinks as it enters the North Atlantic basin, but also by the Azores current closer to the surface (Barton et al., 1998, Martins et al., 2002). The coast line is also different from other coastal jets areas, since its continuity is disrupted by the Gulf of Cadiz. The prevalent boreal summer regional atmospheric flow is also unique there, with two CLLJ features, as mentioned by Ranjha et al. (2013), and not only one, as suggested by Winant et al. (1988). As seen in Fig. 4a the ensemble projected changes of the Iberian Peninsula CLLJ occurrences are, along with the Oman coastal jet, the highest of all coastal jets. The estimated increase in occurrences is accompanied by an expected rise in the jet heights and in the wind speeds at the jet maxima, towards the mid and end 21st century, as seen in Fig. 6a,b histograms. The projected increase in jet heights are highest between 400 to 700 m ASL where, by the end of the 21st century, 50% of the Iberian Peninsula CLLJ occurrences are expected to take place. As in the California CLLJ, a substantial increase in the highest wind speeds is projected to take place, both in mid and end 21st century. The occurrences of the Iberian Peninsula coastal jet are expected to increase substantially in the north sector of the West Coast of Iberia (200–300%, as can be seen in Fig. 6c). A minor (10–20%) increase in the occurrences of the Iberian Peninsula coastal is also projected to occur in the southwest coast of Iberia. In the future the Iberian Peninsula CLLJ wind direction at the jet height will be mostly from north-northeast (around 50% of the times), and almost always from the north-northeasterly sector (Fig. 6d). The height-wind speed combinations depicted in Fig. 8e, show that in the future the Iberian Peninsula coastal jet is expected to be concentrated, between 300 to 500 m ASL with wind speeds of the order of 10 to

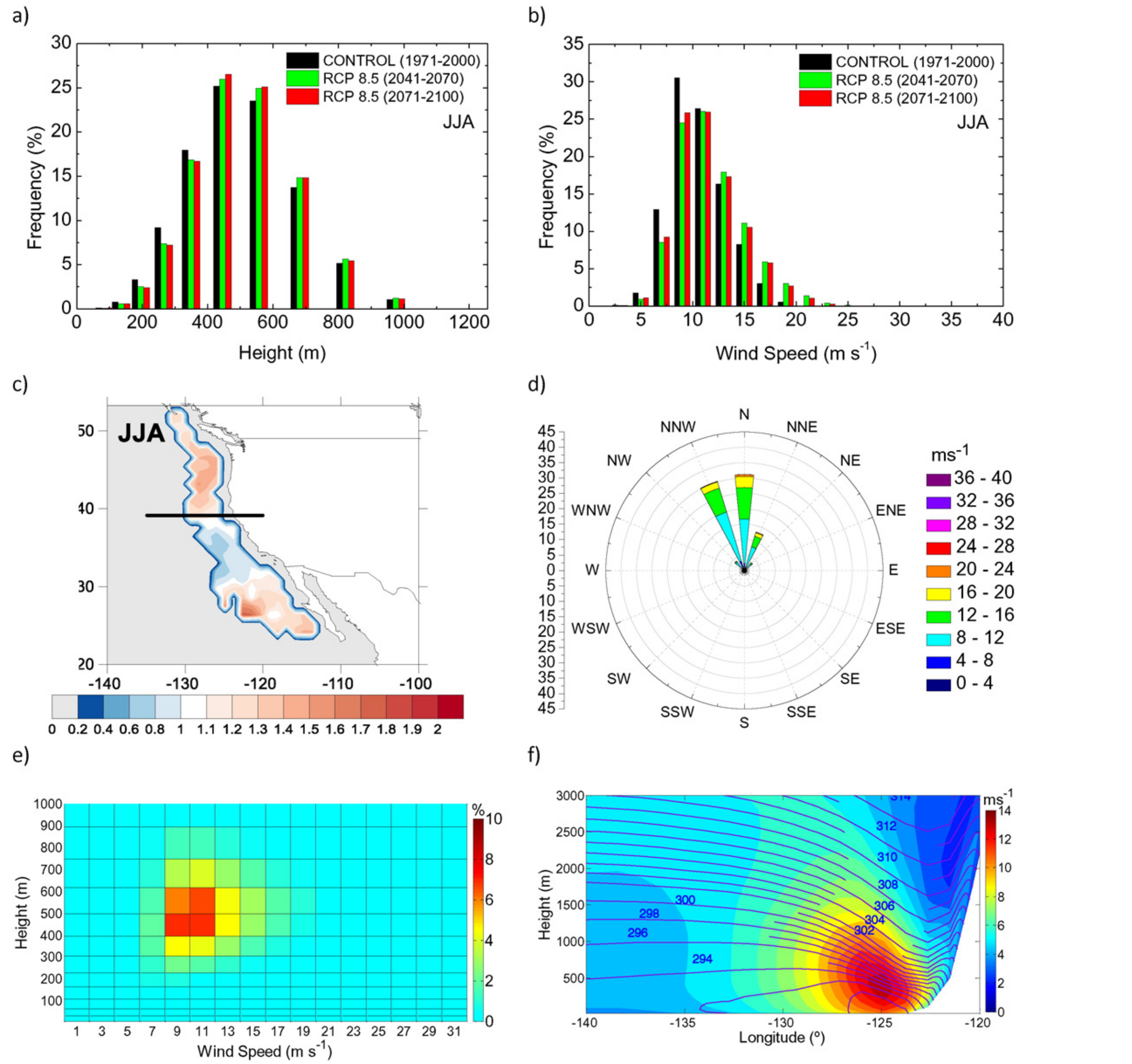

Fig. 5. California CLLJ ensemble control run, mid (2041–2070) and late 21st century (2071–2100) JJA histograms (axis scales vary between panels) of (a) jet heights (m) ASL and (b) wind speed (ms^{-1}) at jet height, when CLLJ occurs, and (c) ratio of late 21st century and present CLLJ frequencies of occurrence (dimensionless; future divided by control run). Late 21st century (2071–2100) characteristics of the California CLLJ (from the ensemble): (d) wind direction histogram (°) at the jet height; (e) jet height-wind histogram (%), and (f) west–east cross section at 37.57°N (along the line in panel c) of mean wind speed (ms^{-1}) when jet occurs (contours) and potential temperature (°K; isentropes in black lines).

14 ms^{-1}. The mean JJA wind speed and potential temperature east–west cross-section (Fig. 6f), along the line in Fig. 6c, reveals a mean jet core at around 400 m, with wind speeds of the order of 12 ms^{-1}, and with a large off-shore span (around 230 km from the coast), clearly lodged at the MABL capping inversion.

4.2.3. North Africa coastal jet

The summer changes of the North Africa CLLJ heights and wind speed maxima, shown in the Fig. 7a,c histograms, reveal a shift towards higher jet heights, but with lower wind speeds, with the exception of extreme wind speed values (higher than 20 ms^{-1}), where an increase is to be expected. The projections of the winter jet heights (Fig. 7b) show an even more pronounced tendency towards higher jets, compared to summer. The future winter wind speed tendency (Fig. 7d) is opposite, with higher wind speeds at the jet height projected to occur in the future. The summer expected North Africa CLLJ occurrences, shown in Fig. 7e, reveal a stagnation close to the coast, but a generalized increase offshore. This increase (of the order of 40 to 60%) can be linked to a future higher off-shore span of the coastal jet. The projected increase in the frequency of the North Africa CLLJ occurrences (Fig. 7f) is considerable higher for the boreal winter, with increases of 200% to 300% or more.

Fig. 8 depicts the projected summer and winter late 21st century North Africa CLLJ characteristics. Regarding the projected wind direction distribution for JJA (Fig. 8a), at the jet height, the wind will be (more than 95% of the times) from north-northeast to northeast sector. During DJF (Fig. 8b) the wind direction is expected to be more from the north-east, although with a higher dispersion from north-northeast to east-northeast. The summer North Africa CLLJ is expected to be mostly concentrated at heights between 500 and 700 m, with wind speeds of the order of 13–14 ms^{-1}, as shown in Fig. 8c. During winter the North Africa CLLJ is expected to occur at lower heights (300–500 m), with wind speeds from 10 to 14 ms^{-1} (Fig. 8d). The cross sections of the JJA and DJF wind speed and potential temperature, averaged for the

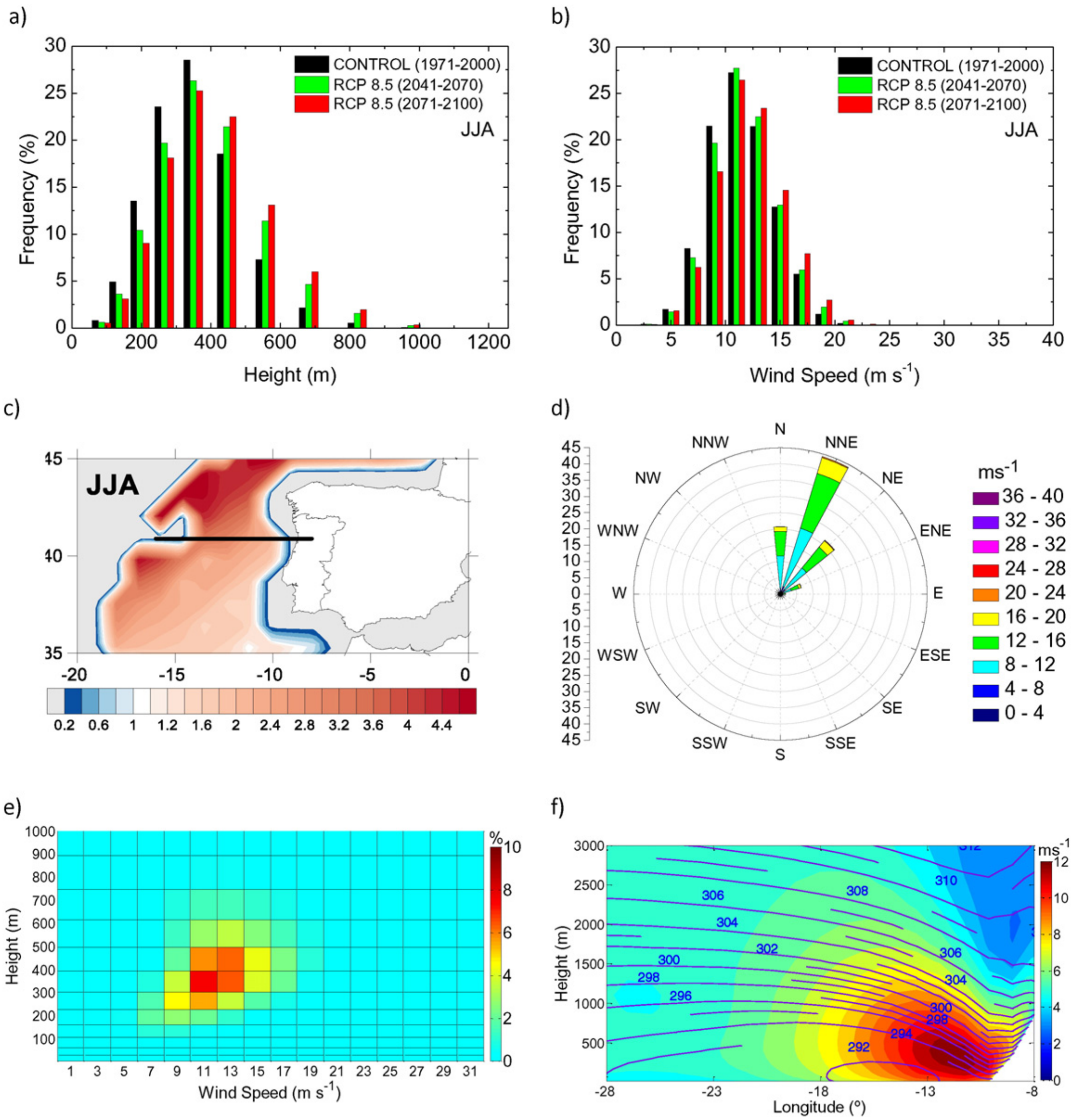

Fig. 6. Same as Fig. 5. but for the Iberian Peninsula CLLJ. West–East cross section at 40.93°N (along the line in panel c).

jet occurrences, shown in Fig. 8e,f (along the black lines in Fig. 7c,d) show a summer mean jet core higher than 500 m ASL, with wind speeds in excess of 12 ms^{-1}, while the winter jet core is considerably lower (less than 300 m ASL) with wind speed lower than 300 m ASL. The off-shore span is comparable between both seasons (of the order of 800 km), although higher in summer.

4.2.4. Oman coastal jet

The Oman CLLJ is the exception to EBC coastal jets. It is found along the southeast coast of the Arabian Peninsula, where the South Asia monsoon circulation plays the same role as the sub-tropical high-pressure circulation does along mid-latitude continental western coasts. Although the impact of a warmer climate in the Oman CLLJ is necessarily linked to future changes in the South Asia Monsoon regime (Annamalai et al., 2013), that is not directly investigated here. The Oman CLLJ ensemble projected changes and its expected future characteristics are presented in Fig. 9. A substantial increase in the occurrence of higher jet heights, as well as of high wind speeds, are to be expected towards the end of the 21st century (Fig. 9a,b). The occurrence of jets higher than 500 m ASL is expected to change from around 35%, in present climate, to more than 50% in the future. On the other hand, the occurrence of jets at heights lower than that value is expected to change from more than 70% in present climate to around 50%. The wind speed is expected to follow a similar pattern, with the increase of the occurrence of high wind speeds at the jet height. Extreme wind speeds (higher than 22 ms^{-1}) are likely to change from about 20% to more than 35%. This increase in extreme future wind speeds can be associated to the projected generalized increase in extreme events in the area, associated with the monsoon, as summarized by the IPCC AR5 (Solomon et al., 2007).

Projected increases of the Oman CLLJ are expected to occur by the end of the 21st century (Fig. 9e), as much as 250%, due to an increase of the off-shore span on the coastal jet towards the Gulf of Oman and Pakistan. A decrease in the Oman CLLJ is to be expected westward, close to the Oman-Yemen border. The projected JJA mean wind direction, at the jet height, is, as expected for the area during the summer monsoon, from southwest to west-southwest, with almost no changes from present climate (not shown). The future concentration of Oman CLLJ occurrences will be at heights 500–600 m, with wind speeds from 18 to 22 ms^{-1} (Fig. 9e). The JJA seasonal cross section (along the

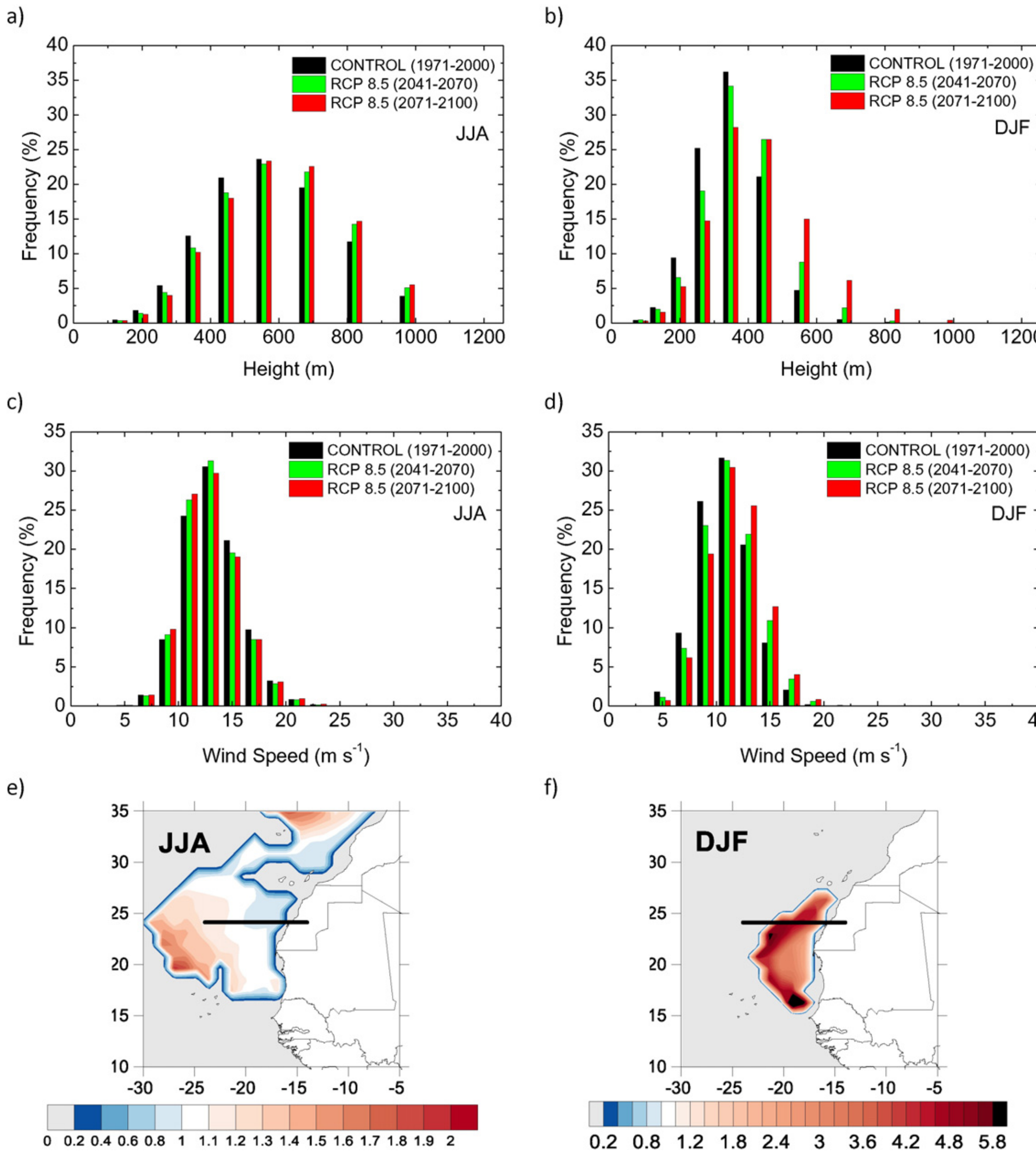

Fig. 7. North Africa CLLJ ensemble control run, mid (2041–2070) and late 21st century (2071–2100) histograms of jet heights (m) ASL for (a) JJA and (b) DJF, and of wind speed (ms^{-1}) at jet height, when CLLJ occurs, for (c) JJA and (d) DJF, and ratio of late 21st century and present CLLJ frequencies of occurrence (dimensionless; future divided by control run), for (e) JJA, and (f) DJF.

black line in Fig. 10c) of the future wind speed an potential temperature (Fig. 9f) clearly shows the height of the jet core, lodged below the temperature inversion (at approximately 700 m ASL), and wind speeds in excess of 20 ms^{-1}. The Oman CLLJ is the one with highest wind speeds at the jet core, as shown by Ranjha et al. (2013, 2015a). The off-shore span of the Oman is of the order of 900 km.

4.2.5. Peru-Chile coastal jet

Figs. 10 and 11 show the DJF and JJA (austral summer and winter) ensemble projected changes, and future characteristics of the Peru-Chile CLLJ, respectively. Following the tendency of the changes of the northern hemisphere coastal jets, the Peru-Chile CLLJ is likely to occur at higher heights in both seasons (Figs. 10a,b), although the projected changes are more significant in JJA. During the austral summer the occurrence of the Peru-Chile CLLJ heights above 550 m ASL are expected to rise. The frequency of occurrence of jet heights above that value is projected to increase from around 33% to close to 40%. The austral winter expected changes, on the other hand, reveal an increase of the occurrence of jet heights above 700 m ALS from 20% to around 35%. Conversely, during JJA, the occurrences of coastal jet heights between 300 m and 700 m, are projected to decrease. As shown above, the projected increase of the coastal jets height, in the northern hemisphere, is accompanied by an upsurge in the occurrence of extreme wind speeds, or at least an increase of the occurrence of the highest wind speeds at the jet heights. This is not the case in the Peru-Chile coastal jet, where the projected changes of future wind speeds are more complicated. In DJF the projected changes clearly indicate that the wind speeds are expected to decrease, i.e., the frequency of occurrence of higher wind speeds (above 16–17 ms^{-1}), is expected to decrease (from around 37% to less than 30%). During JJA, on the other hand, the frequency of occurrence of low wind speeds (lower than 8 ms^{-1}), for the end of the 21st century, is expected to remain almost unchanged. The austral summer and winter Peru-Chile CLLJ occurrences for the end of the 21st century shown in Fig. 10c,d, reveal a generalized increase of coastal jets in the area. During DJF this pattern is more consistent and concentrated off the coast of Peru, from 25°S to around 40°S, with increases of CLLJ

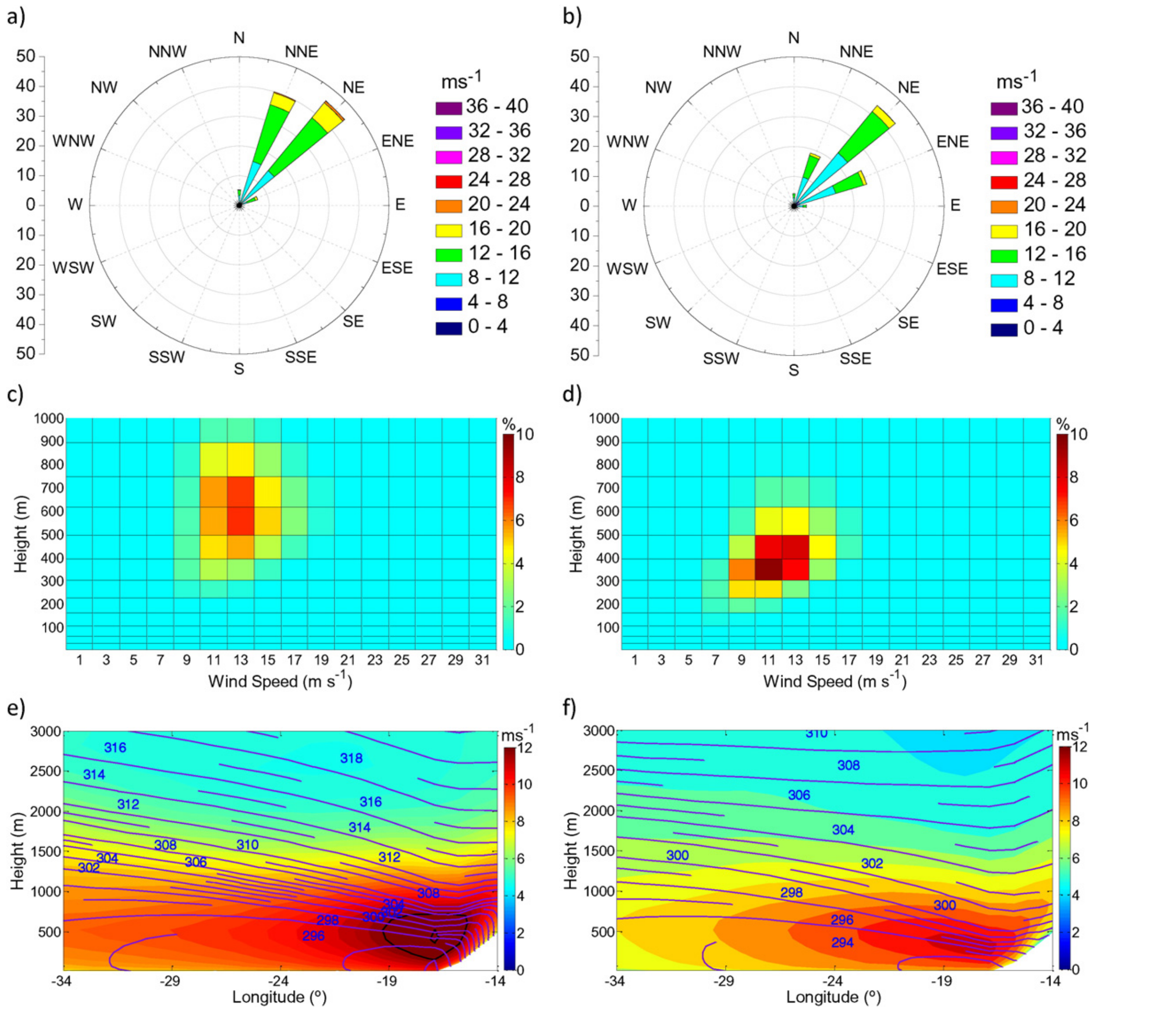

Fig. 8. Late 21st century (2071–2100)) characteristics of the North Africa CLLJ (from the ensemble): wind direction histogram (°) at the jet height for (a) JJA and (b) DJF, jet height-wind histogram (%) for (d) JJA and (f) DJF, and east–west cross sections at 24.11°N (along the lines in Figs. 9e,f) of mean wind speed (ms^{-1}) when jet occurs (contours) and potential temperature (°K; isentropes in black lines) for (e) JJA and (f) DJF.

occurrences away from the coast of the order of the order 50 to 100% (more south). A slight decrease, closer to the coast, is also expected to occur. The northward migration of the synoptic forcing during austral winter, mostly of the South Pacific High, leads to the changes shown in Fig. 10d (increase of 80–100%) of the Peru-Chile CLLJ occurrences along the coast of Chile, as north as offshore Lima. Some modifications (increases offshore and decreases closer to the coast) are also be expected to occur more south, along the central and south shores of Chile.

The yearly latitudinal migration of the Peru-Chile CLLJ is also noticeable in the characteristics of the wind direction at the jet height for the end of the 21st century: mostly southerly winds in DJF (Fig. 11a) and a larger directional dispersion during JJA (Fig. 11b), with wind directions almost evenly distributed within the south to southeast sector. The wind speed-jet heights project concentration of the Peru-Chile CLLJ (Fig. 11c,d) reveal the differences between summer and winter. During summer most occurrences will be concentrated at heights between 300 and 600 m ASL, with wind speeds from 10 to 16 ms^{-1}. A larger vertical dispersion (from 200 to 900 m ASL) is likely to occur during winter, at slightly lower wind speeds (10 to 14 ms^{-1}). The austral summer and winter wind speed and potential temperature cross-sections (Fig. 11e,f) along the black lines shown in Fig. 11e,f show a future PCJ with higher wind speeds and with a larger offshore span than the winter one. The mountain effect on the PCJ is, in this case clear, blocking the perpendicular flow within the MABL completely.

4.2.6. Benguela coastal jet

Figs. 12 and 13 present the ensemble DJF and JJA projected changes for the Benguela CLLJ, and its future seasonal characteristics. The winter and summer projected changes of the jet heights depicted in the histograms shown in Fig. 12a,b reveal, in both cases, projected increases of the jet heights (occurrences higher than 400 m ASL increasing from 60% to close to 75%). A projected decrease (increase) of the high (low) DJF wind speeds is also expected to occur (Fig. 12c). The JJA projected changes show also an increase of the occurrences of low wind speeds (lower than 12 ms^{-1}), and a reduction of the high wind speeds. While the DJF Benguela CLLJ occurrences are projected to increase (Fig. 13e; around 20–30% close to the coast and close to 100% offshore the north coast of Namibia), that is not the case during the austral winter, where the projected changes reveal a slight decrease in the frequency of occurrences along the north Namibian and south Angolan coast.

The characteristics of the future Benguela CLLJ reveal, in spite of its meridional variation, small inter seasonal differences. The summer and winter wind direction distribution (Fig. 13a,b), towards the end of the 21st century, is relatively similar, and is, in both cases, from the

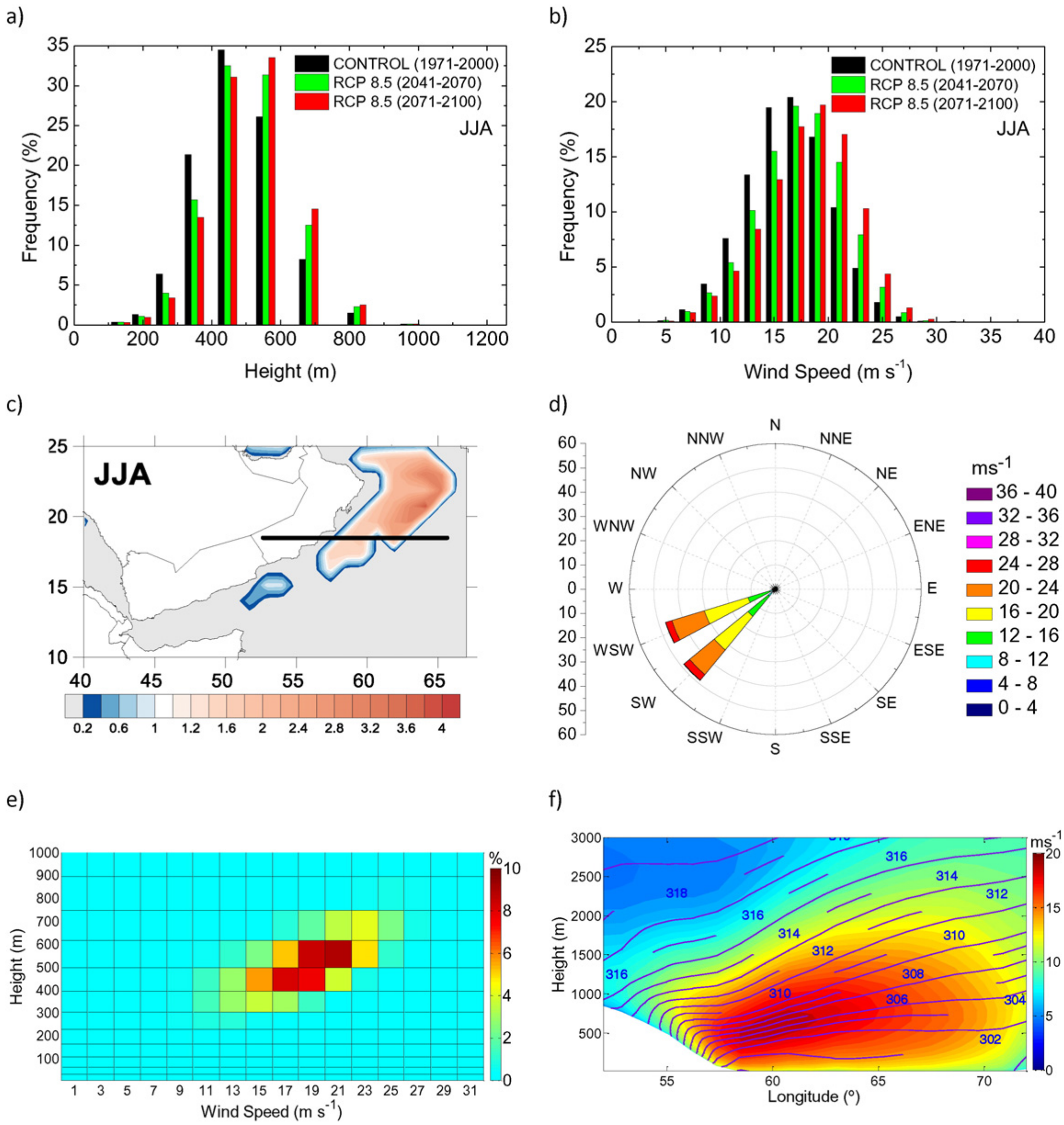

Fig. 9. Same as Fig. 5. but for the Oman CLLJ. West–east cross section at 18.50°N (along the line in panel c). (Histograms axis scales vary between panels a) and b).

south to southeast sector. In the future, the Benguela coastal jet is expected to have most of its occurrences, both during summer and winter (Fig. 13c,d), at heights between 400 m and 600 m ASL, with wind speeds around 10 to 14 ms^{-1}. The wind speed and potential temperature DJF and JJA vertical cross sections of the Benguela CLLJ (along the lines shown in Fig. 12e,f) are also similar, with jet cores constrained within heights lower than 500 m ASL. The mean wind speed at the jet core is expected to be slightly higher during austral summer (about 13 ms^{-1}), and the off-shore span is similar in both cases. This similarity between the summer and winter characteristics of the BCJ was also mentioned by Ranjha et al. (2013).

4.2.7. West Australia coastal jet

The West Australia CLLJ is, after the Iberian Peninsula coastal jet, the one with lower frequencies of occurrence (see Fig. 1b), as previously shown by Ranjha et al. (2013). It also has a well-defined seasonal cycle, being completely absent during austral winter due to the northward migration of the South Indian Ocean high pressure system. The austral summer ensemble projected changes of the West Australia coastal jet and its future characteristics for the end of the 21st century are presented in Fig. 14. The heights of the West Australia CLLJ are projected to increase, with an increase of occurrence of higher jet heights (from 500 m to 800 m ASL) towards the mid and end 21st century, accompanied by less occurrence of lower heights jets (Fig. 14a). The wind speeds at the jet height, on the other hand, are likely to decrease (Fig. 14b), i.e., the occurrence of high wind speeds (higher than 15 ms^{-1}) is expected to decrease (about 7%). This reduction is compensated by an expected increase of the wind speeds from 10 to 15 ms^{-1}, while the low wind speeds are also expected to decrease. The frequencies of occurrence of the West Australia coastal jet (Fig. 14c) by the end of the 21st century are projected to increase. This increase will be less close to the coast (20–30%) and higher off-shore (100% and higher), showing an increase of the offshore span of the West Australia CLLJ.

The projected West Australia CLLJ wind direction at the jet height show a predominance of winds from the south-southeast to southeast sector, with wind speeds mostly within the 12–16 ms^{-1} range (Fig. 14d). The West Australia coastal jet height band is project to occur from 300 m to 500 m ALS, with wind speeds from 10 ms^{-1} to 14 ms^{-1} (Fig. 14e). The east–west vertical cross section of the projected horizontal wind speed (when jet occurs), overlaid with the isentrops

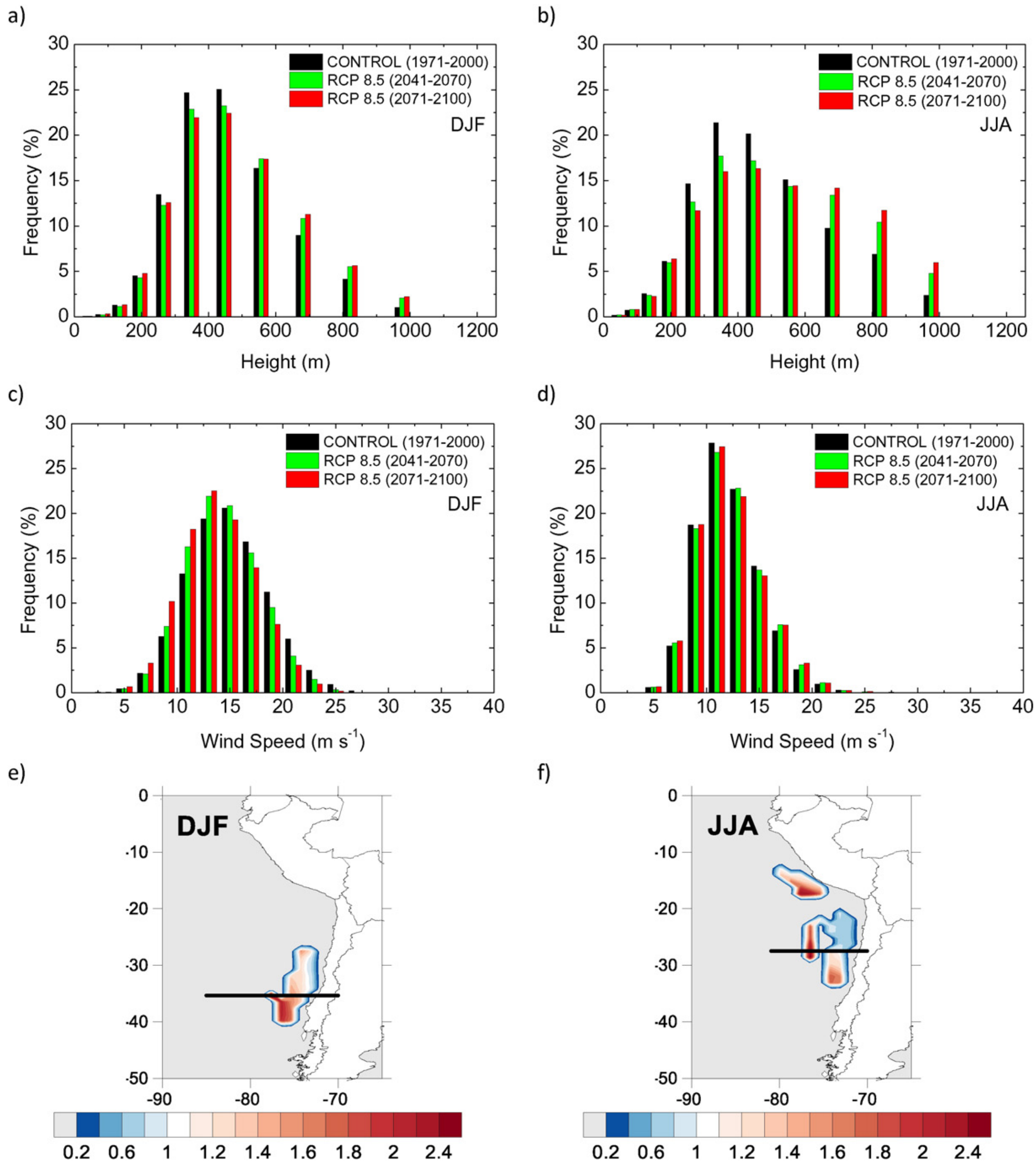

Fig. 10. Peru-Chile CLLJ ensemble control run, mid (2041–2070) and late 21st century (2071–2100) histograms of jet heights (m) ASL for (a) DJF and (b) JJA, and of wind speed (ms^{-1}) at jet height, when CLLJ occurs, for (c) DJF and (d) JJA, and ratio of late 21st century and present CLLJ frequencies of occurrence (dimensionless; future divided by control run), for (e) DJF, and (f) JJA.

(Fig. 14f), reveal a considerable off-shore span (as far as 800 km from the coast).

5. Summary of results and conclusions

Changes in CLLJ climate towards the end of the 21st century were analyzed here from an ensemble based on two EC-Earth CMIP5 runs. These runs were driven by present day and potential future atmospheric conditions under the RCP8.5 IPCC greenhouse gas concentration scenario (Riahi et al., 2011), for the 2006–2100 period. The present climate simulations from the 2-member EC-Earth ensemble covered the period between 1850 and 1855 to 2005, respectively, from which the period between 1971 and 2000 was used as control run. The ensemble control run was evaluated against remote sensing wind observations from the CCMP analyses (Atlas et al., 2011), and against ERA-Interim wind speeds at two pressure levels, with good results, as shown in Tables 1 to 3. The control run global MSLP and 10 m ASL wind speed (and direction) structures (for JJA and DJF; Figs. 2 and 3) were examined. The classification and filtering criteria of CLLJ established by Ranjha et al. (2013) was used to assess the influence of a warmer climate on the global CLLJ frequencies of occurrence by the end of the 21st century, by comparing them to the present climate ones. The ability of the EC-Earth GCM (through the ensemble) to resolve coastal jets along the CLLJ areas was evaluated (Fig. 1), with good results, compared

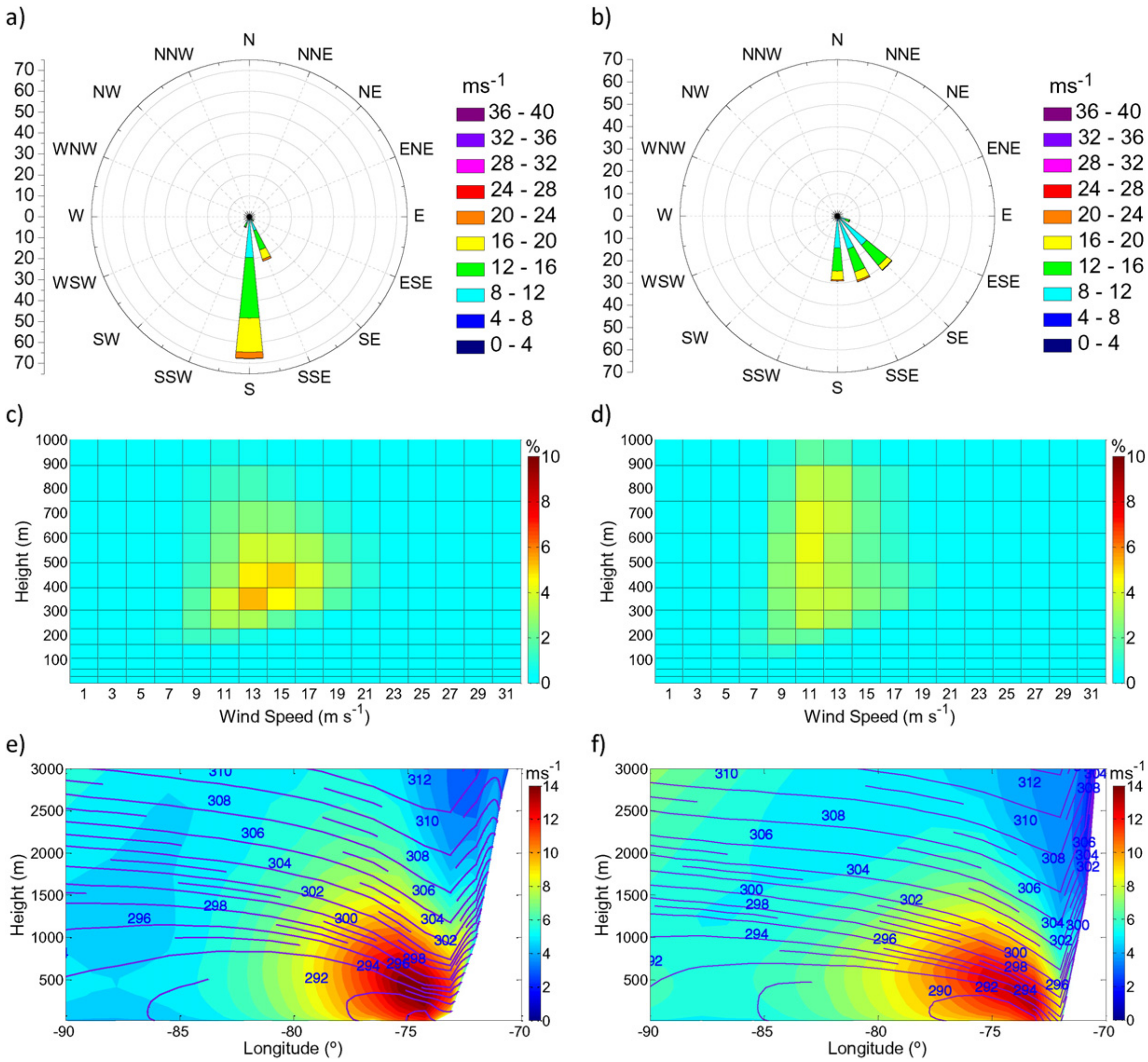

Fig. 11. Late 21st century (2071–2100)) characteristics of the Peru-Chile CLLJ (from the ensemble): wind direction histogram (°) at the jet height for (a) DJF and (b) JJA, jet height-wind histogram (%) for (d) DJF and (f) JJA, and east–west cross sections at 27.48°S (along the lines in Figs. 9e,f) of mean wind speed (ms^{-1}) when jet occurs (contours) and potential temperature (°K; isentropes in black lines) for (e) DJF and (f) JJA.

to the findings of Ranjha et al. (2013), revealing its suitability to resolve and describe CLLJ globally. The projected changes in the global CLLJ climate towards the end of the 21st century were then studied for the 2071–2100 period.

The summary of the projected changes for the seven identified coastal jet regions, for the end of the 21st century, compared with the control run, are depicted in Table 4, where the evolution of the maximum frequency of occurrence, mean jet height and mean wind speed at the jet core, from present to future climates, are presented. These statistics were computed from the grid points where CLLJ occur. During the respective hemisphere summer, the maximum frequency of occurrence of all CLLJ increases, with the exception of the North Africa CLLJ. The mean height of the wind speed maxima increase in all coastal jets in summer but also in winter, for the CLLJ that occur in that season. Although further dedicated research would be needed, this consistent increase in the jet heights could mean an increase in the MABL air temperature and height. This increase in the air temperature could be linked to the generalized projected increase in SST (IPCC AR5, 2013). Nevertheless these variations, in areas of such complexity, could be linked to several other causes. The project changes in the jet wind speeds do not show a coherent pattern. While in boreal summer the wind speed maxima are expected to increase in the Iberian Peninsula and Oman coastal jets (the ones that are expected to have the highest increase in frequency of occurrence), the California and North Africa wind speed maxima have the opposite tendency. On the other hand, in the southern hemisphere during austral summer the Peru-Chile, Benguela, and Western Australia coastal jets are expected to have lower wind speeds at the jet core. The evaluation of the joint changes in the jet heights and wind speeds is important since they can be seen as an indication of changes in the turbulence structure of the MABL. A higher jet with a lower wind speed, considering that there are no changes in the wind speed at the surface, means less wind shear and less mechanical turbulence production, which can have a significant impact in the overall MABL turbulence structure. Projected changes in the subtropical highs (not shown) reveal an increase in the pressure and a slight pole-ward shift (expansion of the Hadley cell, in line with the findings of Johanson and Fu, 2009), but these changes need to be investigated together with the changes of the thermal lows in land and with the associated

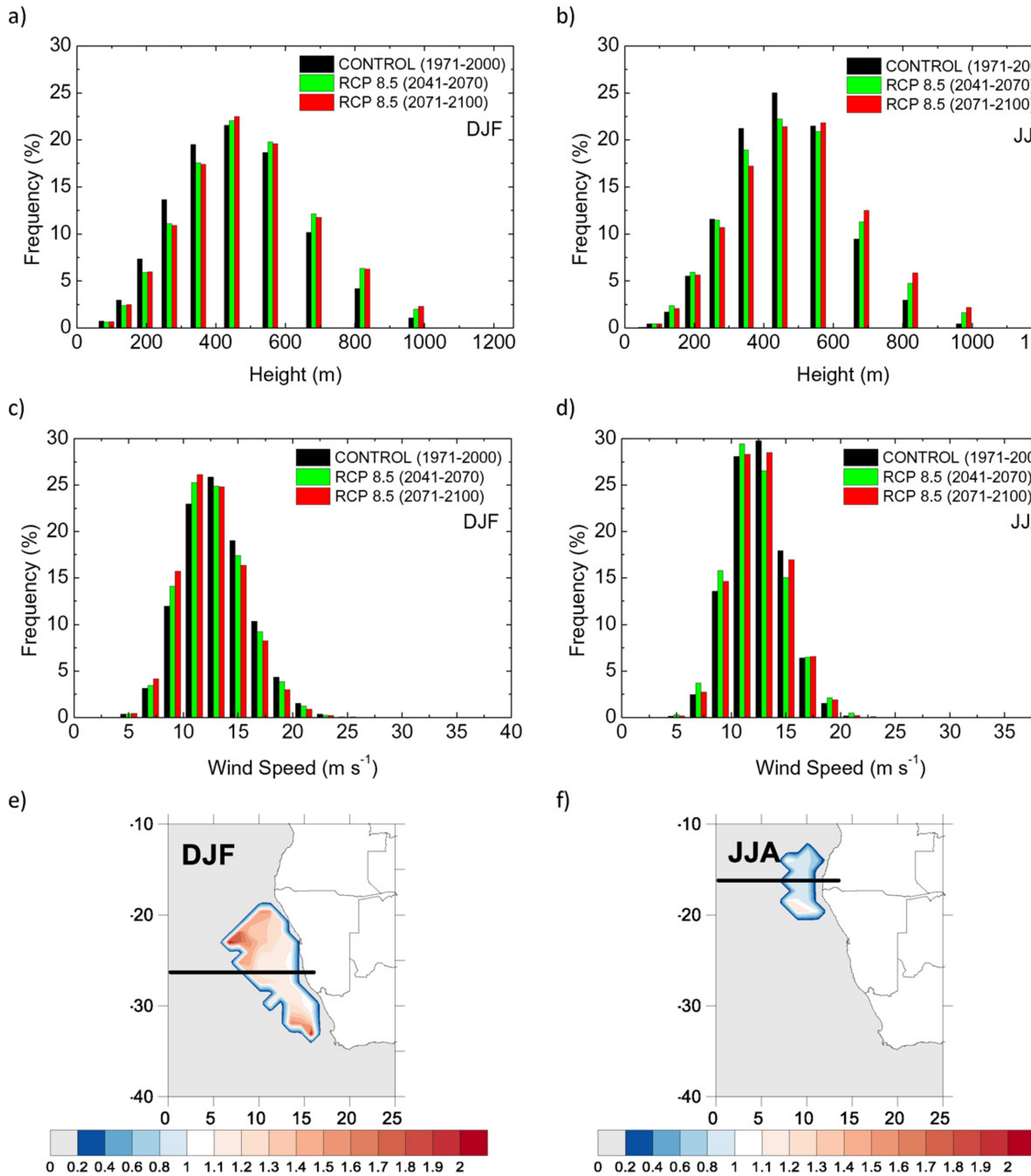

Fig. 12. Same as Fig. 10. but for the Benguela CLLJ.

changes in the along coast wind speed. All these combined changes need a more thorough investigation that should be pursued with higher resolution model simulations, preferably using a coupled model system (like the one used by Miranda et al., 2013, following the findings of Ranjha et al., 2015b) to assess the feedbacks between the ocean and the atmosphere. The projected increases of the Oman CLLJ occurrences (and wind speed in the area; not shown) are corroborated by several other studies, where the intensity of the South Asia Monsoon is to be expected (e.g. Solomon et al., 2007, Loo et al., 2015).

The evolution of the JJA and DJF coastal jets maximum frequency of occurrence, from present to future climate, is shown in Fig. 15.The box plots solid horizontal line represents the median value (50th percentile), while the height of the box shows the inter-quantile range (IQR; between the 75th and the 25th percentiles). The top (bottom) whisker represents the 95th (5th) percentile of the CLLJ frequency of occurrence. The mean are represented by the full squares, and the extreme values (maximum and minimum, and the 99th and 1th percentiles) are also represented, although the minimum values are hard to visualize. The respective summer (boreal and austral) evolution of the extreme values of the frequency of occurrence, points to an increase in all CLLJ. The exception is the North Africa CLLJ, where a projected increase on the 99th percentile is accompanied with a decrease of the maximum frequency of occurrence. Note that the 99th percentile and maximum values are similar in the Oman CLLJ in JJA. In all coastal jets the projected changes in the respective hemisphere summer show an increase of the IQR, with the exception of the California CLLJ, with almost no difference from present to future,

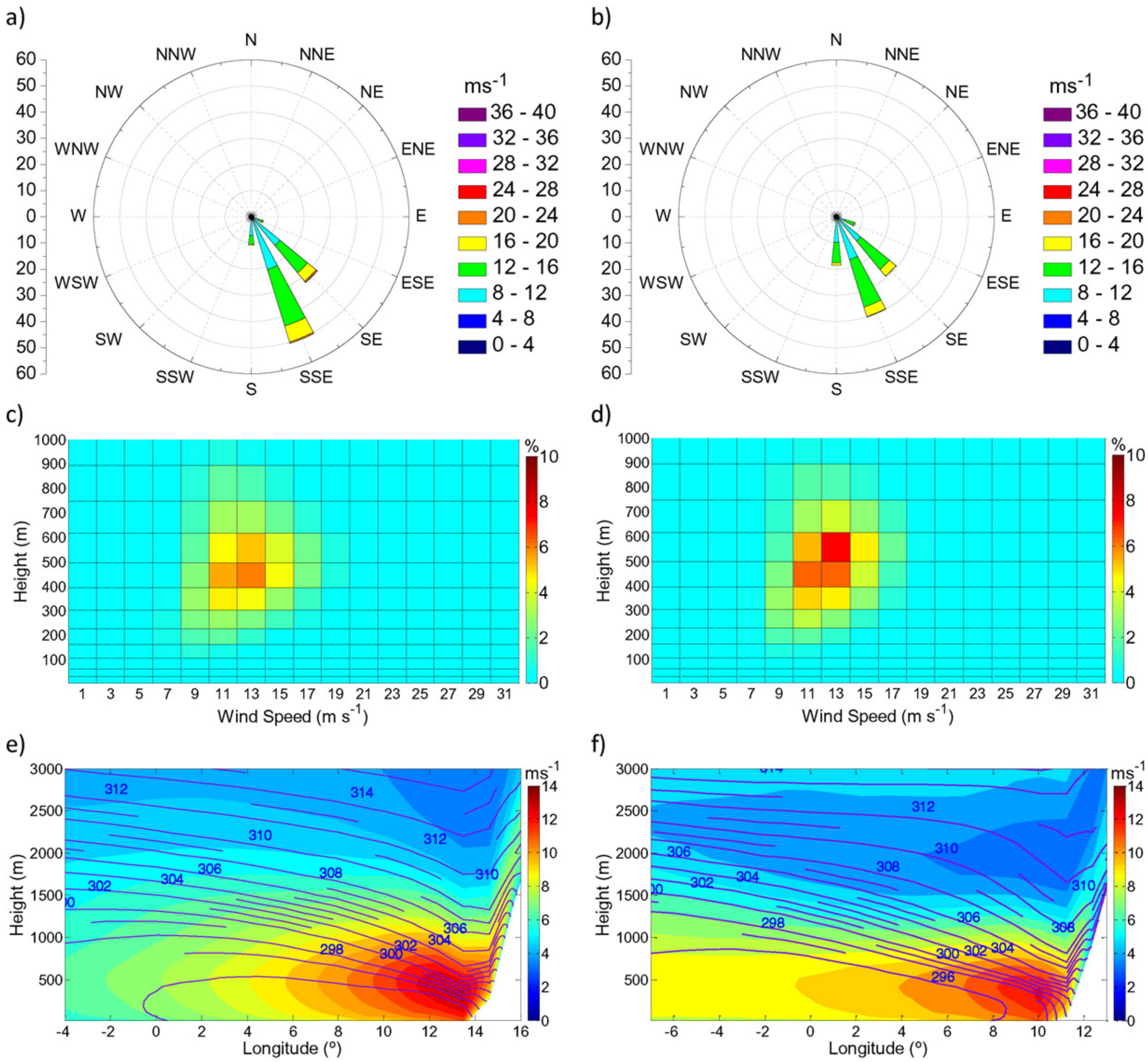

Fig. 13. Same as Fig. 11. but for the Benguela CLLJ. West–east cross sections at 26.36°S and 16.26°S (along the lines in Figs. 14e,f).

and of the North Africa CLLJ where a rather small decrease of the IQR can be observed. The Iberian Peninsula and the Oman coastal jets have the highest projected increases, for the mean, median, 95th percentiles and IQR. The expected changes (increase) of the North Africa CLLJ IQR, in DJF, are significant, going along with the increase of the extreme values of frequency of occurrence. The projected changes of the JJA Peru-Chile and Benguela CLLJ IQR are, on the other hand, rather small, although a decrease in the extreme values is to be expected.

The decadal evolution of the boreal summer Iberian Peninsula and Oman CLLJ, which, from all coastal jets, are the ones expected to present the highest changes in the future, are shown in Fig. 16. The summer Iberian Peninsula CLLJ frequency of occurrence shows a clear positive tendency for the 21st century, particularly after 2070. This positive trend can be seen in all the percentiles, from the 5th to the 99th, as well for the mean values. The IQR also presents an increase, which corresponds to wider frequency of occurrence distributions. A similar behavior can be seen in the decadal evolution of the summer Oman CLLJ. Nevertheless not all percentiles have the same tendency, since, for example, from 2070 to 2090 an increase in the mean frequency of occurrence is to be expected, while during the same period the median will slightly decrease. The variations of the IQR, from the beginning to the end of the 21st century, are also lower, compared to the Iberian Peninsula CLLJ.

For a long time the interest in coastal jets dynamics and in the associated coastal MABL structure, mainly along the coast of California, has been the motivation of several field campaigns (e.g. Zemba and Friehe, 1987, Rahn and Parish, 2000) as well as of several modeling and theoretical studies (e.g. Burk and Thompson, 1996, Ström et al., 2001, Muñoz and Garreaud, 2005). Only recently have climate studies of CLLJ been pursuit (e.g. Ranjha et al., 2013, Soares et al., 2014), but only for present climate.

In spite of the relevance of these coastal wind features in the regional climate, of which the water vapor content in the atmosphere and the correspondent impact on the aridity of the adjacent coastal areas might be seen as the most relevant, the impact of climate change on the CLLJ climate had not been studied before. Coastal jets areas are of vital importance, since besides their relevance from a regional climate point of view, they are also paramount to several economical activities related, for example, to fishing and fish farming, offshore wind farms, or coastal airport management. For this reason the potential impact of changes on the coastal winds pattern along EBC can be considerably large from the

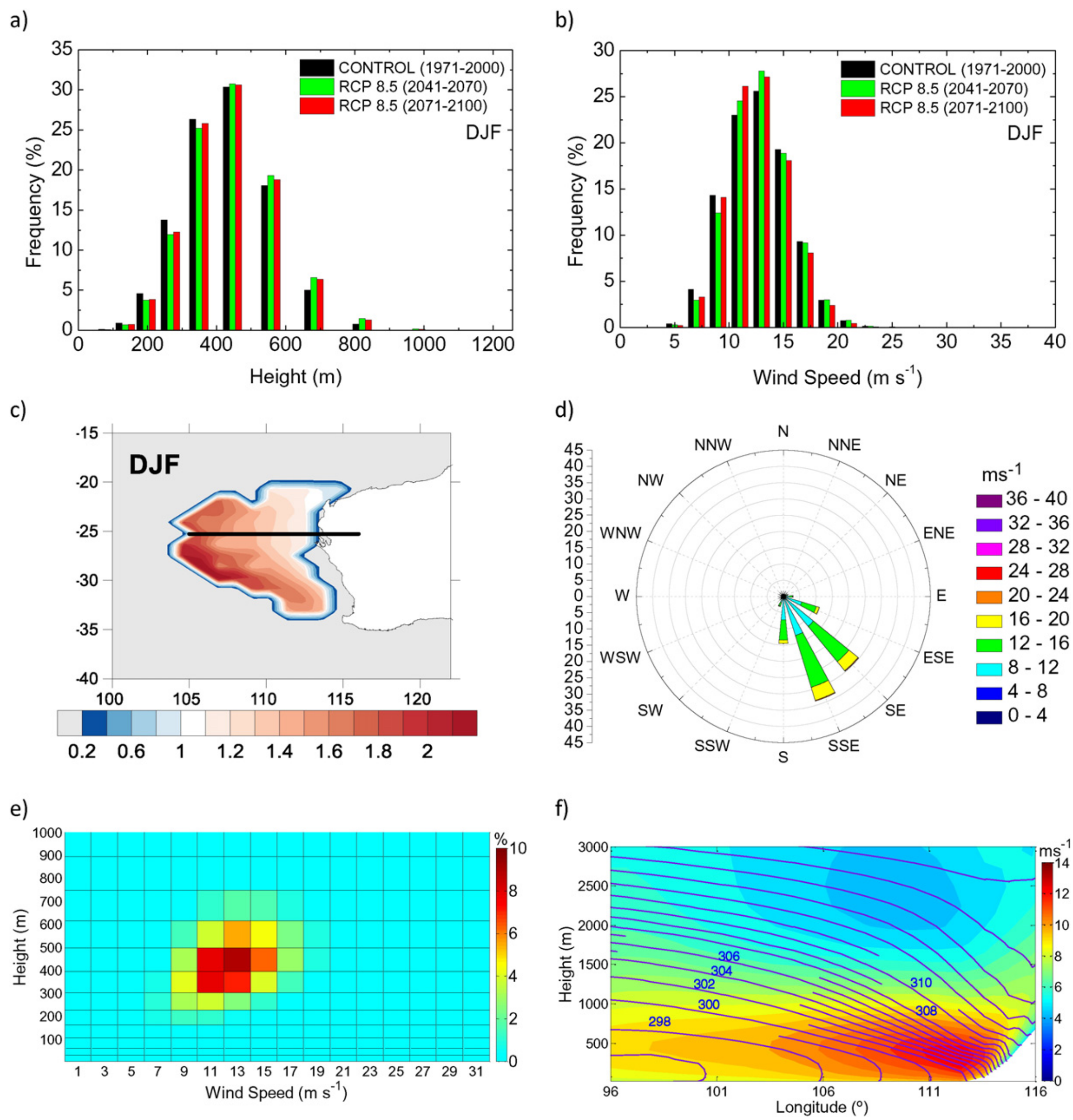

Fig. 14. Same as Fig. 5. but for the West Australia CLLJ and for DJF. West–East cross section at 25.23°S (along the line in panel c). (Histograms axis scales vary between panels a) and b).

economical and societal points of view. The current study presented a diagnostic of the projected impact of a warmer climate in the future CLLJ climate and characteristics. We did not explore the dynamical

Table 3
Same as Table 2 but for the hPa pressure level.

	DJF		JJA	
	S	S < P90	S	S90
CCJ	86.4	93.4	90.0	93.9
IPCJ	80.3	89.5	84.1	84.0
OCJ	85.7	87.3	83.0	90.7
NACJ	91.5	91.6	91.0	86.0
PCCJ	78.9	90.0	86.1	96.3
BCJ	91.9	96.9	84.0	94.8
WACJ	87.7	90.1	83.3	96.3

Table 4
Statistical differences between the JJA and DJF control run (left values) and the late 21st century projections (right values), for the different CLLJ (CCJ — California coastal jet; IPCJ — Iberian Peninsula coastal jet; OCJ — Oman coastal jet; NACJ — North Africa coastal jet; PCCJ — Peru Chile Coastal jet; BCJ — Benguela coastal jet; and WACJ — West Australia coastal jet). The shaded bold values represent projected decreases. The open cells refer to non existing CLLJ.

	JJA			DJF		
	Max. Freq. occurrence (%)	Mean jet height (m)	Mean wind speed (ms^{-1})	Max. Freq. occurrence (%)	Mean jet height (m)	Mean wind speed (ms^{-1})
CCJ	18.15 / 20.09	455.23 / 466.96	11.93 / 11.52	–	–	–
IPCJ	12.45 / 22.64	311.77 / 361.08	11.53 / 12.12	–	–	–
OCJ	32.63 / 50.67	434.13 / 479.53	16.47 / 18.06	–	–	–
NACJ	48.01 / 47.28	517.86 / 555.49	13.18 / 12.98	1.70 / 4.23	309.85 / 384.59	10.85 / 11.66
PCJ	6.94 / 6.11	443.59 / 492.97	12.16 / 12.20	12.33 / 14.35	448.18 / 457.49	14.95 / 13.75
BCJ	9.04 / 7.45	423.46 / 450.20	12.47 / 12.41	21.99 / 23.46	417.79 / 443.41	13.07 / 12.50
WACJ	–	–	–	11.12 / 12.77	384.97 / 400.52	12.70 / 12.57

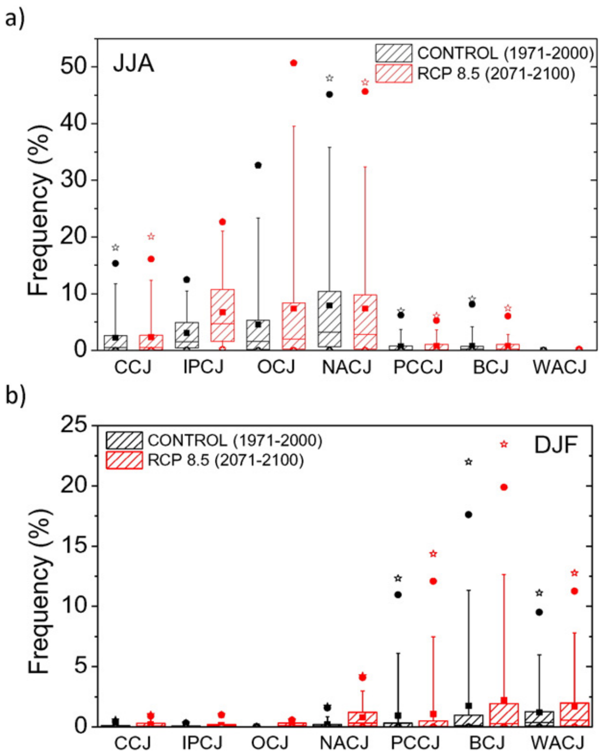

Fig. 15. Statistical differences between the control run (black box plots) and the late 21st century projections (red box plots), for the different CLLJ (CCJ — California coastal jet; IPCJ — Iberian Peninsula coastal jet; OCJ — Oman coastal jet; NACJ — North Africa coastal jet; PCCJ — Peru Chile Coastal jet; BCJ — Benguela coastal jet; and WACJ — West Australia coastal jet), for (a) JJA and (b) DJF. The stars represents the maximum frequency of occurrence, the full circles the 99% percentile, the full squares the mean, the upper (lower) box edge the 75% (25%) percentile, and the horizontal line inside the box the median. The whiskers represent the 95% and the 5% (not seen due to low values) percentiles.

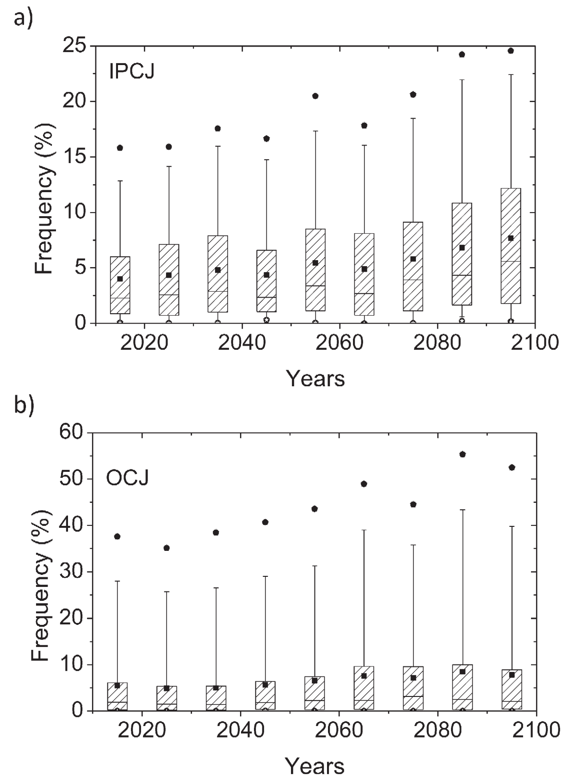

Fig. 16. The stars represents the maximum frequency of occurrence, not seen since they are very close to the full circles that represent the 99% percentile, the full squares represent the mean, and the upper (lower) box edge the 75% (25%) percentile, and the horizontal line inside the box represent the median. The whiskers represent the 95% and the 5% (not seen due to low values) percentiles.

and thermo-dynamical causes of these changes, since they are out of the scope of this study, leaving that for further research.

The relation between higher jet core heights, as most projected changes shown here, seem to be associated to higher MABL atmospheric temperatures, most probably driven by higher SST at the coast. On the other hand, changes in the balance between the ocean temperature at the coast and the temperature in-land, as well as the resulting thermal and pressure gradients, play a decisive role on the local wind speed, which needs to be further investigated. Regional climate modeling studies at higher resolutions, for each coastal jet areas, necessarily at higher resolution than the ensemble, need to be pursued. Despite the fact that, up to the authors' knowledge, no other study has addresses the impact of climate change in the CLLJ occurrences and future features before, the ensemble used here can be seen as short, leaving room for potential uncertainties. For this reason a larger ensemble of the projected impact of climate change on the coastal jets occurrences and future characteristics is needed. The authors plan to pursue this study in the near future using CMIP6 EC-Earth runs, at higher resolution and with a considerably larger ensemble.

Acknowledgments

This work was pursuit in the framework of the SHARE project (RECI/GEO-MET/0380/2012) and of the SOLAR project (PTDC/GEOMET/7078/2014), both financed by the Portuguese Foundation for Science and Technology. Rita Cardoso was supported by EUPORIAS — 7th Framework Program for Research, Grant Agreement 308291. All authors are part of UID/GEO/50019/2013.

References

Annamalai, H., Hafner, J., Sooraj, K.P., Pillai, P., 2013. Global warming shifts the monsoon circulation drying South Asia. J. Climate 26, 2701–2718.
Atlas, R., Hoffman, R.N., Ardizzone, J., Leidner, S.M., Jusem, J.C., co-authors, 2011. A cross-calibrated, multiplatform ocean surface wind velocity product for meteorological and oceanographic applications. Bull. Am. Meteorol. Soc. 92, 157–174.
Bakun, A., 1990. Global climate change and intensification of coastal ocean upwelling. Science 247, 198–201.
Barton, E., et al., 1998. The transition zone of the canary current upwelling region. Prog. Oceanogr. 41, 455–504.
Beardsley, R.C., Dorman, C.E., Friehe, C.A., Rosenfield, L.K., Wyant, C.D., 1987. Local atmospheric forcing during the coastal ocean dynamics experiment 1: a description of the marine boundary layer and atmospheric conditions over a northern California upwelling region. J. Geophys. Res. 92, 1467–1488.
Burk, S.D., Thompson, W.T., 1996. The summertime low-level jet and marine boundary 656 layer structure along the California coast. Mon. Weather Rev. 124, 668–686.
Burk, S.D., Haack, T., Samelson, R.M., 1999. Mesoscale simulation of supercritical, subcritical, and transcritical flow along coastal topography. J. Atmos. Sci. 56, 2780–2795.
Cardoso, R.M., Soares, P.M.M., Miranda, P.M.A., Belo-Pereira, M., 2013. WRF high resolution simulation of Iberian mean and extreme precipitation climate. Int. J. Climatol. 33, 2591–2608.
Dee, D.P., Uppala, S., 2009. Variational bias correction of satellite radiance data in the ERA-interim reanalysis. Q. J. R. Meteorol. Soc. 135, 1830–1841.
Dee, D.P., Uppala, S.M., Simmons, A.J., Berrisford, P., Poli, P., co-authors, 2011. The ERA-interim reanalysis: configuration and performance of the data assimilation system. Q. J. R. Meteorol. Soc. 137, 553–597.
Demarcq, H., 2009. Trends in primary production, sea surface temperature and wind in upwelling systems (1998–2007). Prog. Oceanogr. 83 (1–4), 376–385.
Findlater, J., 1969. A major low level current near the Indian Ocean during northern 686 summer. Q. J. R. Meteorol. Soc. 95, 362–380.
Garreaud, R.D., Muñoz, R.C., 2005. The low-level jet off the West Coast of subtropical South America: structure and variability. Mon. Weather Rev. 133, 2246–2261.
Gergana, Y., Nowaczyk, N.R., Mingram, J., Dulski, P., Schettler, G., Negendank, J.F.W., Liu, J., Sigman, D.M., Peterson, L.C., Haug, G.H., 2007. Influence of the intertropical convergence zone on the east Asian monsoon. Nature 445, 74–77.
Hazeleger, W., et al., 2010. EC-earth: a seamless earth system prediction approach in action. BAMS 91, 1357–1363.
Hazeleger, W., Wang, X., Severijns, C., Stefanescu, S., Bintanja, R., Sterl, A., Wyser, K., Semmler, T., Yang, S., van den Hurk, B., van Noije, T., van der Linden, E., van der

Wiel, K., 2013. EC-earth V2.2: description and validation of a new seamless earth system prediction model. Clim. Dyn. 39, 2611–2629.
IPCC, 2013. In: Stocker, T.F., Qin, D., Plattner, G.-K., Tignor, M., Allen, S.K., Boschung, J., Nauels, A., Xia, Y., Bex, V., Midgley, P.M. (Eds.), Climate Change 2013: The Physical Science Basis. Contribution of Working Group I to the Fifth Assessment Report of the Intergovernmental Panel on Climate Change. Cambridge University Press, Cambridge, United Kingdom and New York, NY, USA http://dx.doi.org/10.1017/CBO9781107415324 (1535 pp.).
Janssen, P.A.E.M., 2004. The Interaction of Ocean Waves and Wind. Cambridge University Press (300 pp.).
Johanson, C.M., Fu, Q., 2009. Hadley cell widening: model simulations versus observations. J. Climate 22, 2713–2725. http://dx.doi.org/10.1175/2008JCLI2620.1.
Knutti, R., 2008. Why are climate models reproducing the observed global surface warming so well? Geophys. Res. Lett. 35, L18704. http://dx.doi.org/10.1029/2008GL034932.
Koracin, D., Dorman, C., 2001. Marine atmospheric boundary layer divergence and clouds along California in June 1996. Mon. Weather Rev. 129, 2040–2055.
Loo, Y.Y., Billa, L., Singh, A., 2015. Effect of climate change on seasonal monsoon in Asia and its impact on the variability of monsoon rainfall in Southeast Asia. Geosci. Front. 6 (6), 817–823.
Martins, C.S., Hamann, M., Fuiza, A.F.G., 2002. Surface circulation in the eastern north Atlantic from drifters and altimetry. J. Geophys. Res. 107, 3217.
Miranda, P.M.A., Alves, J.M.R., Serra, N., 2013. Climate change and upwelling: response of Iberian upwelling to atmospheric forcing in a regional climate scenario. Clim. Dyn. 40, 2813–2824.
Muñoz, R.C., Garreaud, R.D., 2005. Dynamics of the low-level jet off the West Coast of subtropical South America. Mon. Weather Rev. 133, 3661–3677.
Narayan, N., Paul, A., Mulitza, S., Schulz, M., 2010. Trends in coastal upwelling intensity. Ocean Sci. 6, 815–823.
Nicholson, S.E., 2010. A low-level jet along the Benguela coast, an integral part of the Benguela current ecosystem. Clim. Chang. 99, 613–624.
Nuss, W.A., Bane, J., Thompson, W., Dorman, C., Ralph, M., co-authors, 2000. Coastally trapped wind reversals: a new level of understanding from the experiment on coastally trapped disturbances. Bull. Am. Meteorol. Soc. 81, 719–743.
Olivier, J., 1995. Spatial distribution of fog in the Namib. J. Arid Environ. 29 (2), 129–138.
Parish, T.R., 2000. Forcing of the summertime low-level jet along the California coast. J. Appl. Meteorol. 39, 2421–2433.
Pauly, D., Christensen, V., 1995. Primary production required to sustain global fisheries. Nature 374, 255–257.
Perkins, S.E., Pitman, A.J., Holbrook, N.J., McAneney, J., 2007. Evaluation of the AR4 climate models' simulated daily maximum temperature, minimum temperature, and precipitation over Australia using probability density functions. J. Clim. 20, 4356–4376.
Ranjha, R., Svensson, G., Tjernström, M., Semedo, A., 2013. Global distribution and seasonal variability of coastal low-level jets derived from ERA-interim reanalysis. Tellus A 65, 20412.
Ranjha, R., Tjernström, M., Semedo, A., Svensson, G., Cardoso, R.M., 2015a. Structure and variability of the Oman coastal low-level jet under revision in. Tellus A 67, 25285.
Ranjha, R., Tjernström, M., Svensson, G., Semedo, A., 2015b. Modeling coastal low-level wind-jets: does horizontal resolution matter? (in press) Meteorog. Atmos. Phys.
Riahi, et al., 2011. RCP8.5 — a scenario of comparatively high greenhouse gas emissions. Clim. Chang. 109 (1–2), 33–57.
Snyder, M.A., Sloan, L.C., Diffenbaugh, N.S., Bell, J.L., 2003. Future climate change and upwelling in the California current. Geophys. Res. Lett. 30, 1823.
Soares, P.M.M., Cardoso, R.M., Miranda, P.M.A., Medeiros, J., Belo-Pereira, M., co-authors, 2012. WRF high resolution dynamical downscaling of ERA-interim for Portugal. Clim. Dyn. 39, 2497–2522.
Soares, P.M.M., Cardoso, R.M., Semedo, A., Chinita, M.J., Ranjha, R., 2014. Climatology of Iberia coastal low-level wind jet: WRF high resolution results. Tellus A 66, 22377.
Solomon, S., Qin, D., Manning, M., Chen, Z., Marquis, M., Averyt, K., Tignor, M., Miller Jr., H.L., 2007. Climate Change 2007: The Physical Science Basis. Cambridge University Press (996 pp.).
Sterl, A., Bintanja, R., Brodeau, L., Gleeson, E., Koenigk, T., Schmith, T., Semmler, T., Severijns, C., Wyser, K., Yang, S., 2012. A look at the ocean in the EC-earth climate model. Clim. Dyn. 39 (11), 2631–2657.
Ström, L., Tjernström, M., Rogers, D.P., 2001. Observed dynamics of topographically forced flow at cape Mendocino during coastal waves 1996. J. Atmos. Sci. 58 (953–731).
Tjernström, M., Koračin, D., 1995. Modeling the impact of marine stratocumulus on boundary layer structure. J. Atmos. Sci. 52, 863–878.
Tjernström, M., Grisogono, B., 2000. Simulations of supercritical flow around points and capes in the coastal atmosphere. J. Atmos. Sci. 57, 108–135.
Warner, T.T., 2004. Desert Meteorology. Cambridge University Press, Boston, MA (595 pp.).
Winant, C.D., Dorman, C.E., Friehe, C.A., Beardsley, R.C., 1988. The marine layer off northern California: an example of supercritical channel flow. J. Atmos. Sci. 45, 3588–3605.
Zemba, J., Friehe, C.A., 1987. The marine boundary layer jet in the coastal ocean dynamics experiment. J. Geophys. Res. 92, 1489–1496.